Annu. Rev. Nucl. Part. Sci. 2002. 52:115–51
doi: 10.1146/annurev.nucl.52.050102.090641

DOUBLE BETA DECAY

Steven R. Elliott
Department of Physics, University of Washington, Seattle, Washington 98195; e-mail: sre@u.washington.edu

Petr Vogel
Department of Physics, California Institute of Technology, Pasadena, California 91125; e-mail: pxv@caltech.edu

Key Words neutrinoless decay, massive Majorana neutrinos, matrix elements, experimental search for $\beta\beta(0\nu)$ decay

PACS Codes 11.30.Fs, 14.60.−z, 23.40.−s

■ **Abstract** The motivation, present status, and future plans of the search for $\beta\beta(0\nu)$ decay are reviewed. Recent observations of neutrino oscillations encourage the hope that $\beta\beta(0\nu)$ decay corresponding to the neutrino mass scale suggested by oscillations, $m_\nu \approx 50$ meV, actually exists. The challenges to achieve the sensitivity corresponding to this mass scale, and plans to overcome them, are described.

CONTENTS

1. INTRODUCTION

Since the last *Annual Review* article on double beta decay (1), published in 1994, there have been several exciting developments. Most significantly, the neutrino oscillation experiments convincingly show that neutrinos have a finite mass.

However, in oscillation experiments only the differences in squares of the neutrino masses, $\Delta m^2_{ij} \equiv |m^2_i - m^2_j|$, can be measured. Nevertheless, a lower limit on the absolute value of the neutrino mass scale, $m_{\rm scale} = \sqrt{\Delta m^2}$, has been established in this way. Its existence, in turn, is causing a renaissance of enthusiasm in the double beta decay community, because the next generation of experiments is expected to reach a sensitivity corresponding to this mass scale. Below, we review the current status of double beta decay and the effort devoted to reach the required sensitivity. But before proceeding, we briefly summarize the achievements of the neutrino oscillation searches and the role of the search for the neutrinoless double beta decay in the elucidation of the pattern of neutrino masses and mixing. In these introductory remarks, we use the established terminology, some of which is only defined later in the text.

There is a consensus that the measurement of atmospheric neutrinos by the SuperKamiokande collaboration (2) can be interpreted only as a consequence of the nearly maximal mixing between ν_μ and ν_τ neutrinos (i.e., $\sin^2 2\theta_{\rm atm} \sim 1.0$) with the corresponding mass squared difference $\Delta m^2_{\rm atm} \sim 3 \times 10^{-3}$ eV^2, i.e., $m_{\rm scale} \sim$ 50 meV. This finding is supported by the K2K experiment (3) that uses an accelerator ν_μ beam pointing toward the SuperKamiokande detector 250 km away, and is in accord with the earlier findings of the Kamiokande (4), IMB (5), and Soudan (6) experiments. Several large long-baseline experiments are being built to further elucidate this discovery and determine the corresponding parameters more accurately.

At the same time, in the "solar neutrino puzzle," which has been with us for over 30 years since the pioneering chlorine experiment of Davis (7), the interpretation of the measurements in terms of oscillations between the ν_e and some combination of active (i.e., ν_μ and ν_τ) neutrinos now seems inescapable. That conclusion is particularly supported by the results of the SNO experiment (8) and SuperKamiokande (9), along with the earlier solar neutrino flux determination in the chlorine and gallium (10, 11) experiments. The values of the corresponding oscillation parameters remain uncertain. Several "solutions" are possible, although the so-called large-mixing-angle (LMA) solution with $\sin^2 2\theta_{\rm sol} \sim 0.8$ (but $\sin^2 2\theta_{\rm sol} < 1$) and $\Delta m^2_{\rm sol} \sim 5 \times 10^{-5}$ eV^2 is preferred at present. Again, the continuing and soon-to-be-operational experiments, such as KamLAND and Borexino, aim to clarify which of the possible solutions is the correct one.

The pattern of neutrino mixing is further simplified by the constraint due to the CHOOZ and PALO VERDE reactor neutrino experiments (12, 13), which indicate that the third mixing angle, θ_{13}, is small, $\sin^2 2\theta_{13} \leq 0.1$.

The oscillation experiments cannot determine the absolute magnitude of the masses. In particular, they cannot at this stage separate two rather different scenarios: the hierarchical pattern of neutrino masses, in which the neutrino masses m_i and/or m_j are of similar magnitude as $\sqrt{\Delta m^2_{ij}}$, and the degenerate pattern, in which all $m_i \gg \sqrt{\Delta m^2_{ij}}$. It is likely that the search for the neutrinoless double beta decay, reviewed here, will help in the foreseeable future to establish the correct mass pattern and to determine, or at least strongly constrain, the absolute neutrino mass scale.

Moreover, the oscillation results tell us nothing about the properties of neutrinos under charge conjugation. Whereas the charged leptons are Dirac particles, distinct from their antiparticles, neutrinos may be the ultimate neutral fermions, as envisioned by Majorana, identical with their antiparticles. That fundamental distinction becomes important only for massive particles. Neutrinoless double beta decay, $\beta\beta(0\nu)$, proceeds only when neutrinos are massive Majorana particles; hence, observing $\beta\beta(0\nu)$ would establish neutrinos as such fermions.

According to the standard electroweak model, neutrinos are massless, and the total lepton number and the individual flavor lepton numbers are conserved. Most people believe that the standard model, despite its enormous success, is incomplete, and physics beyond the standard model is being actively pursued on many fronts. The observation of neutrino mass and oscillation is a clear example of a phenomenon at variance with the standard model. Further elucidation of various aspects of neutrino mass will help point us toward the proper extension of the standard model.

Double beta decay is a rare transition between two nuclei with the same mass number (A) that changes the nuclear charge (Z) by two units. The decay can proceed only if the initial nucleus is less bound than the final one, and both must be more bound than the intermediate nucleus (or the decay to the intermediate nucleus must be highly hindered, as in ^{48}Ca). These conditions are fulfilled in nature for many even-even nuclei, and only for them. Typically, the decay can proceed from the ground state (spin and parity always 0^+) of the initial nucleus to the ground state (also 0^+) of the final nucleus, although the decay into excited states (0^+ or 2^+) is in some cases also energetically possible.

The two-neutrino decay, $\beta\beta(2\nu)$,

$$(Z, A) \rightarrow (Z + 2, A) + e_1^- + e_2^- + \overline{\nu}_{e1} + \overline{\nu}_{e2}, \qquad 1.$$

which involves the transformation of two neutrons into protons, conserves not only electric charge but also lepton number. (Analogous decays, involving transformation of two protons into neutrons, are also sometimes possible. We concentrate here, however, on the decays $2n \rightarrow 2p$, for which there are more candidate nuclei and usually larger Q values.)

On the other hand, the neutrinoless decay, $\beta\beta(0\nu)$,

$$(Z, A) \rightarrow (Z + 2, A) + e_1^- + e_2^-, \qquad 2.$$

violates lepton number conservation and is therefore forbidden in the standard electroweak theory. In addition, there can be transitions $\beta\beta(0\nu,\chi)$ in which a light neutral boson χ, a majoron postulated in various extensions of the standard electroweak theory (14), is emitted:

$$(Z, A) \rightarrow (Z + 2, A) + e_1^- + e_2^- + \chi. \qquad 3.$$

The interest in double beta decay spans more than six decades. Already in 1937, Racah (15), following the fundamental suggestion of Majorana (16), discussed the

possibility of a neutrinoless transformation of two neutrons into two protons plus two electrons. Even earlier, Goeppert-Mayer (17) evaluated the decay rate of the $\beta\beta(2\nu)$ mode and realized that the corresponding half-life could exceed 10^{20} y. And Furry, shortly afterward (18), estimated that the $\beta\beta(0\nu)$ decay should be much faster than the $\beta\beta(2\nu)$ decay. That conclusion, however, had to be revised with the discovery of parity nonconservation in weak interactions. Thus, the stage was set for the realization that the observation of the $\beta\beta(0\nu)$ decay would establish that the neutrino is a massive Majorana particle.

Numerous earlier reviews of double beta decay include the classics by Primakoff & Rosen (19), Haxton & Stephenson (20), and Doi et al. (21). More recent reviews, besides Reference (1), include those by Boehm & Vogel (22) (which lists the phase-space integrals), Suhonen & Civitarese (23) (which deals mostly with the nuclear matrix elements), Faessler & Šimkovic (24), Vergados (25), and Klapdor-Kleingrothaus (26). A rather complete list of experimental data can be found in the papers by Tretyak & Zdesenko (27, 28). The *Review of Particle Physics* regularly lists the most important double beta decay experimental data (29). For a recent review of the whole field of neutrino mass and oscillations, see Reference (30).

It is easy to distinguish the three decay modes ($\beta\beta(2\nu)$, $\beta\beta(0\nu)$, and $\beta\beta(0\nu, \chi)$) by the shape of the electron sum energy spectra, which are determined by the phase space of the outgoing light particles. Figure 1 illustrates these spectra for the $\beta\beta(2\nu)$ and $\beta\beta(0\nu)$ modes. In the 2ν decay, the summed kinetic energy K_e of the two electrons displays a broad maximum below half the endpoint energy. In contrast, in the $\beta\beta(0\nu)$ mode, the two electrons carry the full available kinetic energy (the nuclear recoil is negligible for all practical purposes) and the spectrum is therefore a single peak at the endpoint. In the majoron decay (omitted from Figure 1 for simplicity), the electron spectrum is again continuous, but the maximum is shifted higher, above the halfway point, as required by the three-light-particle phase space.

The inset in Figure 1 illustrates in detail the expected spectra near the endpoint, where the $\beta\beta(2\nu)$ decay represents the ultimate background to the search for the $\beta\beta(0\nu)$ mode (see Section 4.2.4 for discussion).

The $\beta\beta(2\nu)$ decay mode is an allowed process. However, since it is a second-order semileptonic weak decay, its lifetime, proportional to $(G_F \cos\theta_C)^{-4}$, is very long. Observing $\beta\beta(2\nu)$ decay presents a formidable challenge, since it must be detected despite the inevitable presence of traces of radioisotopes that have similar decay energy but lifetimes more than 10 orders of magnitude shorter. Nevertheless, at present, that challenge has been met and the $\beta\beta(2\nu)$ decay has been positively identified in a number of cases. Observing the $\beta\beta(2\nu)$ decay not only confirms that the necessary background suppression has been achieved but also constrains the nuclear models needed to evaluate the corresponding nuclear matrix elements.

Hand in hand with the observation of the $\beta\beta(2\nu)$ decays, the experiments became sensitive to longer and longer half-lives of the $\beta\beta(0\nu)$ decay mode. Because the $\beta\beta(0\nu)$ rate is proportional to the square of effective neutrino mass, the improvements led to correspondingly improved limits on the mass. This is illustrated

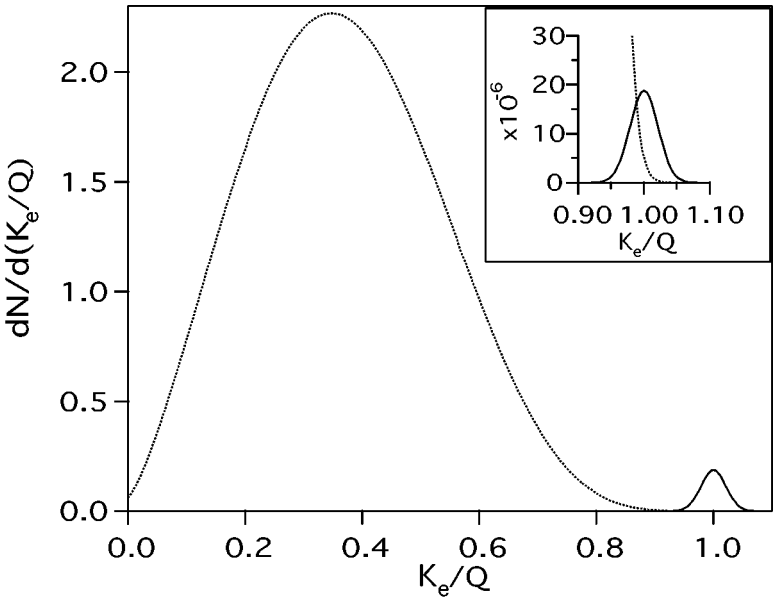

Figure 1 Illustration of the spectra of the sum of the electron kinetic energies K_e (Q is the endpoint) for the $\beta\beta(2\nu)$ normalized to 1 (dotted curve) and $\beta\beta(0\nu)$ decays (solid curve). The $\beta\beta(0\nu)$ spectrum is normalized to 10^{-2} (10^{-6} in the inset). All spectra are convolved with an energy resolution of 5%, representative of several experiments. However, some experiments, notably Ge, have a much better energy resolution.

in Figure 2, which shows an essentially exponential improvement, by more than a factor of four per decade, of the corresponding limits. If this trend continues, we expect to reach the neutrino mass scale suggested by the oscillation experiments in 10–20 years. Given the typical lead time of the large particle physics experiments, the relevant double beta decay experiments should begin the "incubation" process now.

2. NEUTRINO MASS: THEORETICAL ASPECTS

2.1. Majorana and Dirac Neutrinos

Empirically, neutrino masses are much smaller than the masses of the charged leptons with which they form weak isodoublets. Even the mass of the lightest charged lepton, the electron, is at least 10^5 times larger than the neutrino mass constrained by the tritium beta decay experiments. The existence of such large factors is difficult to explain unless one invokes some symmetry principle. The assumption that neutrinos are Majorana particles is often used in this context. Moreover, many theoretical constructs invoked to explain neutrino masses lead to the conclusion that neutrinos are massive Majorana fermions.

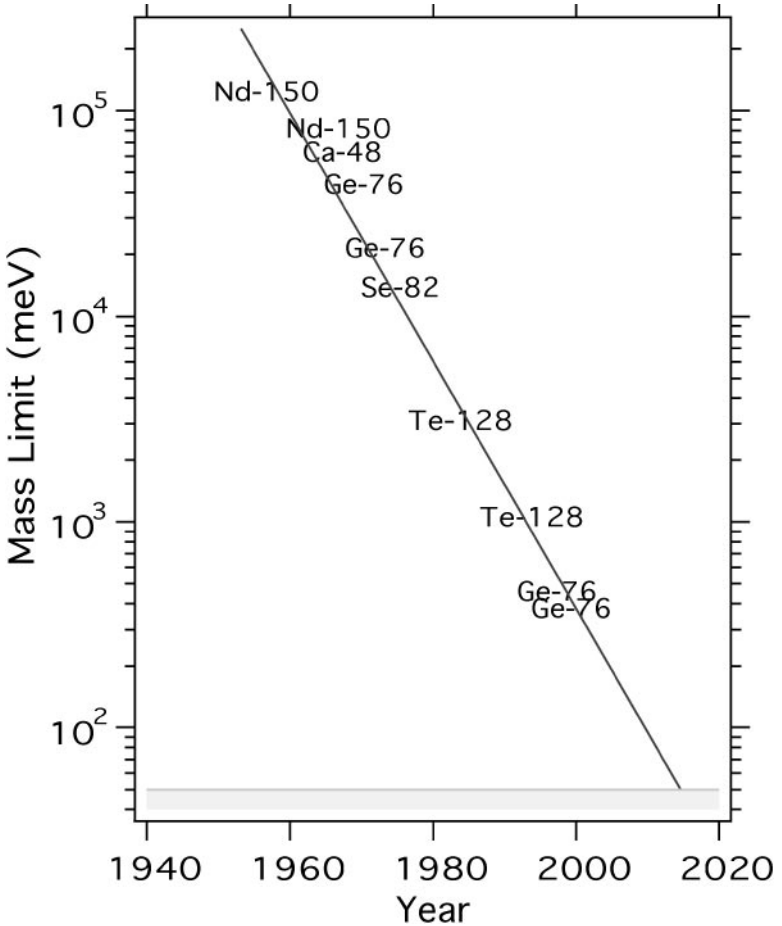

Figure 2 "Moore's law" of $\beta\beta(0\nu)$ decay: the limit of the effective neutrino mass versus time. The corresponding experiments are denoted by the symbol for the initial nucleus. The uncertainty in the nuclear matrix elements is not included in this illustration. The gray band near the bottom indicates the neutrino mass scale $\sqrt{\Delta m^2_{\rm atm}}$.

Majorana particles are identical with their own antiparticles whereas Dirac particles can be distinguished from their antiparticles. This implies that Majorana fermions are two-component objects whereas Dirac fermions are four-component. In order to avoid confusion and to derive the formula for the $\beta\beta(0\nu)$ rate mediated by the exchange of massive Majorana neutrinos, we briefly discuss the formalism needed to describe them (for more details see, e.g., References 21, 31–33).

Massive fermions are usually described by the Dirac equation, in which the chirality eigenstates ψ_R and ψ_L are coupled and form a four-component object of

mass m:

$$i\left(\hat{\sigma}^{\mu}\partial_{\mu}\right)\psi_R - m\psi_L = 0, \quad i\left(\sigma^{\mu}\partial_{\mu}\right)\psi_L - m\psi_R = 0, \qquad 4.$$

where $\hat{\sigma}^{\mu} = (\sigma^0, \vec{\sigma})$, $\sigma^{\mu} = (\sigma^0, -\vec{\sigma})$, and $(\sigma^0, \vec{\sigma})$ are the Pauli matrices. As written, $\psi_{L(R)}$ are two-component spinors; the usual four-component bispinors are defined as

$$\Psi = \begin{pmatrix} \psi_R \\ \psi_L \end{pmatrix}; \quad \Psi_R = \begin{pmatrix} \psi_R \\ 0 \end{pmatrix}; \quad \Psi_L = \begin{pmatrix} 0 \\ \psi_L \end{pmatrix}, \qquad 5.$$

where $\Psi_{L(R)}$ are just the chiral projections of Ψ, i.e., the eigenstates of $P_{L(R)} = (1 \mp \gamma_5)/2$.

However, Majorana's suggestion (16) allows one to describe those massive fermions that have no conserved additive quantum numbers as either two-component ψ_R (mass m) or ψ_L (mass m') that obey independent equations:

$$i\left(\hat{\sigma}^{\mu}\partial_{\mu}\right)\psi_R - m\epsilon\psi_R^* = 0; \quad i\left(\sigma^{\mu}\partial_{\mu}\right)\psi_L + m'\epsilon\psi_L^* = 0, \qquad 6.$$

where $\epsilon = i\sigma_y$.

The Majorana fields can be also expressed in the four-component form:

$$\Psi_L(x) = \begin{pmatrix} -\epsilon\psi_L^*(x) \\ \psi_L(x) \end{pmatrix} \quad \text{and/or} \quad \Psi_R(x) = \begin{pmatrix} \psi_R(x) \\ \epsilon\psi_R^*(x) \end{pmatrix}. \qquad 7.$$

Such a four-component notation is useful to express the charged weak current in a compact form. It is then clear that the Dirac field Ψ, Equation 5, is equivalent to a pair of Majorana fields with $m = m'$ and $\psi_L = \epsilon\psi_R^*$.

The four-component Majorana fields, Equation 7, are self-conjugate, $\Psi^c_{L(R)}(x) = \Psi_{L(R)}(x)$, where charge conjugation is defined as $\Psi^c_{L(R)}(x) = i\gamma^2\gamma^0\bar{\Psi}^T_{L(R)}$. The fields $\Psi_L(x)$ and $\Psi_R(x)$ are eigenstates of *CP* with opposite eigenvalues.

The Lorentz-invariant mass term in the neutrino Langrangian can appear in three forms:

$$M_D\left[\bar{\nu}_R\nu_L + (\bar{\nu}_L)^c\nu_R^c\right], \quad M_L\left[(\bar{\nu}_L)^c\nu_L + \bar{\nu}_L\nu_L^c\right], \quad M_R\left[(\bar{\nu}_R)^c\nu_R + \bar{\nu}_R\nu_R^c\right], \quad 8.$$

where we have introduced the notation $\nu_{L(R)}$ for the corresponding neutrino annihilation operators. The first expression in Equation 8 is the Dirac mass term (with the mass parameter M_D), which requires the existence of both chirality eigenstates ν_L and ν_R and conserves the lepton quantum number. The second and third mass terms are Majorana mass terms that violate lepton number and can be present even without ν_R (for the term with mass parameter M_L) or ν_L (for the term with mass parameter M_R). In general, all three terms might coexist, and then the mass Langrangian must be diagonalized, resulting in two generally nondegenerate mass eigenvalues for each flavor. [That is the situation with the generic see-saw mass (35), where it is assumed that $M_R \gg M_D \gg M_L \sim 0$, and the light neutrino acquires the mass $m_\nu \sim M_D^2/M_R$.]

Let us consider now the general situation with N flavors of the left-handed neutrinos ν_L and also N flavors of the right-handed neutrinos ν_R. The most general Lorentz-invariant mass term of the neutrino Langrangian then has the form

$$\mathcal{L}_M = -\frac{1}{2}((\overline{\nu}_L)^c \;\; \overline{\nu}_R)\mathcal{M}\begin{pmatrix}\nu_L \\ \nu_R^c\end{pmatrix} + \text{h.c.}, \quad \mathcal{M} = \begin{pmatrix}\mathcal{M}_L & \mathcal{M}_D^T \\ \mathcal{M}_D & \mathcal{M}_R\end{pmatrix}, \qquad 9.$$

where ν_L and ν_R are column vectors of dimension N. Here $\mathcal{M}_L$ and $\mathcal{M}_R$ are symmetric $N \times N$ matrices (Majorana masses for the left- and right-handed neutrinos) and $\mathcal{M}_D$ is an arbitrary and generally complex $N \times N$ matrix.

The mass matrix $\mathcal{M}$, with real positive eigenvalues $m_1, \ldots, m_{2N}$, is diagonalized by the $2N \times 2N$ unitary matrix

$$\begin{pmatrix}\nu_L \\ \nu_R^c\end{pmatrix} = \begin{pmatrix}U \\ V\end{pmatrix}\Phi_L. \qquad 10.$$

The general mixing matrices U and V have N rows and $2N$ columns, and Φ_L is a column vector of dimension $2N$ of Majorana-like objects (31). On the other hand, if none of the states ν_R exist, or if $\mathcal{M}_R$ is so large that the corresponding states need not be considered, only $\mathcal{M}_L$ is relevant, and only the $N \times N$ mixing matrix U is needed to diagonalize the mass term (and Φ_L has then only N components, naturally).

Let us consider in more detail the latter case, when only $\mathcal{M}_L \neq 0$. The $N \times N$ unitary mixing matrix U contains N^2 real parameters. However, N of them correspond to unphysical phases; there are $N(N-1)/2$ angles and $N(N-1)/2$ physically relevant phases describing possible *CP* violations. (For a discussion of parameter counting, see Reference (31).) In the oscillation experiments that violate only the flavor lepton number, while conserving the total lepton number (such as $\nu_e \to \nu_\mu$ or $\nu_\mu \to \nu_\tau$), one can determine, in principle, all angles and $(N-1)(N-2)/2$ phases. These phases, common to the Dirac and Majorana neutrinos, describe *CP* violation responsible for the possible differences of the oscillation probabilities $\nu_\ell \to \nu_{\ell'}$ and $\overline{\nu}_\ell \to \overline{\nu}_{\ell'}$.

The remaining $N-1$ phases affect only neutrino-oscillation–like processes (in which neutrinos are created in the charged-current weak processes and absorbed again in charged current) that violate the total lepton number, such as the $\beta\beta(0\nu)$ decay. Such phases are physically significant only for Majorana neutrinos; they are unphysical for Dirac neutrinos. This is so because, for Majorana neutrinos, one cannot perform the transformation $\nu_i \to \nu_i' = e^{i\alpha_i}\nu_i$, which would violate the self-conjugation property.

In principle, the distinction between Dirac and Majorana neutrinos affects other processes as well, such as the angular distribution of νe scattering or photon polarization in the $\nu_i \to \nu_j + \gamma$ decay. However, the "Practical Dirac-Majorana Confusion Theorem" (35) states that the distinction vanishes for $m_\nu \to 0$, which makes it essentially unobservable in these cases.

2.2. $\beta\beta(0\nu)$ Decay Rate and Majorana Mass

Here we consider only the simplest case of the left-handed $V - A$ weak currents and light massive Majorana neutrinos. This is the case of current interest provided the neutrino mass revealed in the oscillation experiments is of Majorana character. (The more general expressions can be found in other reviews, e.g., References (20, 21). For a recent formulation of the general problem, see Reference (36).)

The differential decay rate of the $\beta\beta(0\nu)$ process, Equation 2, is (21)

$$d\Gamma_{0\nu} = 2\pi \sum_{\text{spin}} |R_{0\nu}|^2 \delta(\epsilon_1 + \epsilon_2 + E_f - M_i) \frac{\mathrm{d}\vec{p}_1}{(2\pi)^3} \frac{\mathrm{d}\vec{p}_2}{(2\pi)^3}, \qquad 11.$$

where $\epsilon_{1(2)}$ and $\vec{p}_{1(2)}$ are total energies and momenta of the electrons and $E_f(M_i)$ is the energy of the final (mass of the initial) nuclear state. The quantity $R_{0\nu}$ is the reaction amplitude to be evaluated in the second-order pertubation theory with respect to the weak interactions.

The lepton part of $R_{0\nu}$, involving the emission and reabsorption of the Majorana neutrino of mass m_j, is

$$-i \int \frac{d^4q}{(2\pi)^4} e^{-iq(x-y)} \overline{e}(x) \gamma_\rho P_L \frac{q^\mu \gamma_\mu + m_j}{q^2 - m_j^2} P_L \gamma_\sigma e^c(y), \qquad 12.$$

where $P_L = (1 - \gamma_5)/2$, $\overline{e}(x)$ and $e^c(y)$ are the electron creation operators, and q is the momentum-transfer four-vector. Because γ_μ anticommutes with γ_5, this amplitude is proportional to m_j and the term with $q^\mu \gamma_\mu$ vanishes. After integration over the energy of the virtual neutrino dq^0, the denominator $q^2 - m_j^2$ is replaced by its residue ω_j/π, where $\omega_j = \sqrt{\vec{q}^2 + m_j^2}$. The amplitude is therefore proportional to $m_j/\omega_j \ll 1$ for light neutrinos.

The remaining integration over the virtual neutrino momentum $3\vec{q}$ leads to the appearance of the neutrino potentials

$$H_k(r, A_k) = \frac{2R_N}{\pi r} \int_0^\infty dq \frac{q \sin(qr)}{\omega(\omega + A_k)},$$
$$A_{1(2)} = E_m - (M_i + M_f)/2 \pm (\epsilon_1 - \epsilon_2)/2, \qquad 13.$$

where 1 and 2 label the emitted electrons, E_m is the excitation energy of the intermediate nucleus, M_f is the mass of the final nucleus, and r is the distance between the two neutrons that are changed into protons. The factor R_N, the nuclear radius, is introduced in order to make the potentials H_k dimensionless. In the case of the $\beta\beta(0\nu)$ decay, one can use the closure approximation, replacing E_m with an appropriate mean value. (This is justified because we expect the momentum of the virtual neutrino to be determined by the uncertainty relation $q \sim 1/r \sim 100$ MeV; thus, the variation of E_m from state to state can be neglected.) The contributions of the two electrons are then added coherently, and thus the neutrino potential to use is

$$H(r) = [H_1(r, A_1) + H_2(r, A_2)]/2 \approx H(r, \bar{A}), \qquad 14.$$

where $\bar{A} = \bar{E}_m - (M_i + M_f)/2$ and $\bar{E}_m$ is the average energy of the intermediate nucleus. The potential $H(r)$ only very weakly depends on m_j as long as the neutrino mass is less than ~10 MeV.

For the ground-state–to–ground-state transitions, i.e., $0_i^+ \rightarrow 0_f^+$, it is enough to consider s-wave outgoing electrons and to use the nonrelativistic approximation for the nucleons. The nuclear part of the amplitude then turns into a sum of the Gamow-Teller and Fermi nuclear matrix elements, where the superscript 0ν signifies the presence of the neutrino potential $H(r)$:

$$|M^{0\nu}| \equiv M_{\rm GT}^{0\nu} - \frac{g_V^2}{g_A^2} M_{\rm F}^{0\nu} = \langle f | \sum_{lk} H(r_{lk}, \bar{A}) \tau_l^+ \tau_k^+ \left(\vec{\sigma}_l \cdot \vec{\sigma}_k - \frac{g_V^2}{g_A^2} \right) | i \rangle. \quad 15.$$

The summation is over all nucleons, $|f\rangle$ ($|i\rangle$) are the final (initial) nuclear states, and $g_V (g_A)$ are the vector (axial vector) coupling constants. Such an expression is now analogous to the allowed approximation of the ordinary beta decay.

Thus, in the approximations described above, which are quite accurate, the transition amplitude for a Majorana neutrino of mass m_j is simply a product of m_j and the above combination of the nuclear matrix elements. The mixing amplitude U_{ej} appears in both vertices, so the physical $\beta\beta(0\nu)$ reaction amplitude contains the factor U_{ej}^2 (not $|U_{ej}|^2$) and is proportional to the factor

$$\langle m_\nu \rangle = \left| \sum_j m_j U_{ej}^2 \right|, \quad 16.$$

where the sum is only over light neutrinos with $m_j < 10$ MeV. (For heavier neutrinos, one cannot neglect the mass in the neutrino propagator; see Equation 12.) The quantity $\langle m_\nu \rangle$ is the effective neutrino mass. Because U_{ej}^2 appears in $\langle m_\nu \rangle$ (and not $|U_{ej}|^2$), the effective neutrino mass depends on the Majorana phases discussed above.

To obtain the decay rate, the reaction amplitude has to be squared and multiplied by the corresponding phase-space integral, which in this case (see Equation 11) is simply the two-electron phase-space integral proportional to

$$G^{0\nu} \sim \int F(Z, \epsilon_1) F(Z, \epsilon_2) p_1 p_2 \epsilon_1 \epsilon_2 \delta(E_0 - \epsilon_1 - \epsilon_2) d\epsilon_1 d\epsilon_2, \quad 17.$$

where E_0 is the available energy (the sum electron kinetic energy peak is at $Q = E_0 - 2m_e$). $F(Z, \epsilon)$ is the usual Fermi function that describes the Coulomb effect on the outgoing electron.

Summarizing, if the $\beta\beta(0\nu)$ decay is mediated by the exchange of a light massive Majorana neutrino (the assumption that we wish to test), the half-life is

$$\left[T_{1/2}^{0\nu}(0^+ \rightarrow 0^+) \right]^{-1} = G^{0\nu}(E_0, Z) \left| M_{\rm GT}^{0\nu} - \frac{g_V^2}{g_A^2} M_{\rm F}^{0\nu} \right|^2 \langle m_\nu \rangle^2, \quad 18.$$

where $G^{0\nu}$ is the exactly calculable phase-space integral, $\langle m_\nu \rangle$ is the effective

neutrino mass, and $M_{\rm GT}^{0\nu}$, $M_{\rm F}^{0\nu}$ are the nuclear matrix elements, defined in Equation 15. The way these nuclear matrix elements are evaluated, and the associated uncertainty, is discussed in the next section. [As explained above, the neutrino mass appears in the amplitude in the combination $m_j/\omega_j \ll 1$; the denominator ω_j has been absorbed in the neutrino potential $H(r)$.]

Thus, if an upper limit on $\beta\beta(0\nu)$ rate is experimentally established, and the nuclear matrix elements are known, one can deduce the corresponding upper limit on $\langle m_\nu \rangle$. On the other hand, if $\beta\beta(0\nu)$ is observed, one can deduce the appropriate value of $\langle m_\nu \rangle$. That procedure is justified, however, only if the exchange of the light Majorana neutrino, discussed above, is indeed the mechanism responsible for the decay. There is no way to determine the mechanism when only the decay rate is known. However, a general theorem (37) states that once $\beta\beta(0\nu)$ has been observed, in gauge theories the Majorana neutrino mass necessarily arises. But the magnitude of the corresponding neutrino mass is difficult to estimate if the exchange of a virtual light Majorana neutrino is not the dominant mechanism of the $\beta\beta(0\nu)$ decay.

2.3. $\beta\beta(0\nu)$ Decay and Oscillation Parameters

Let us assume that there are N massive Majorana neutrinos $\nu_i, i = 1, \ldots, N$. In that case, the weak eigenstate neutrinos ν_e, ν_μ, and ν_τ can be expressed as superpositions of ν_i using the $3 \times N$ mixing matrix $U_{\ell i}$. In particular, electron neutrinos are then superpositions,

$$\nu_e = \sum_i^N U_{ei}\,\nu_i, \qquad 19.$$

and the rate of the $\beta\beta(0\nu)$ decay is proportional to (see Equation 18 and References 38, 39)

$$\langle m_\nu \rangle^2 = \left| \sum_i^N U_{ei}^2 m_i \right|^2 = \left| \sum_i^N |U_{ei}|^2 e^{\alpha_i} m_i \right|^2, \quad (\text{all } m_i \geq 0). \qquad 20.$$

This quantity depends, as indicated, on the $N-1$ Majorana phases $\alpha_i/2$ of the matrix U discussed in Subsection 2.1, which are irrelevant in neutrino oscillation experiments that do not change the total lepton number.

If CP is conserved, $\alpha_i = k\pi$, but generally any values of α_i are possible. Thus, $\langle m_\nu \rangle$ could be complex and cancellations in the sum are possible. [For example, a Dirac neutrino corresponds to a pair of degenerate Majorana neutrinos with $e^{\alpha_i} = \pm 1$, whose contributions to $\langle m_\nu \rangle$ exactly cancel. More generally, some models, such as the Zee model (40), postulate that $\langle m_\nu \rangle = 0$.]

Whereas the quantity $\langle m_\nu \rangle$ depends on the unknown phases α_i, the upper and lower limits of $\langle m_\nu \rangle$, $\langle m_\nu \rangle_{\rm max}$ and $\langle m_\nu \rangle_{\rm min}$, depend only on the absolute values of the mixing angles (41),

$$\langle m_\nu \rangle_{\rm max} = \sum_i |U_{ei}|^2 m_i, \;\; \langle m_\nu \rangle_{\rm min} = \max[(2|U_{ei}|^2 m_i - \langle m_\nu \rangle_{\rm max}), 0]. \qquad 21.$$

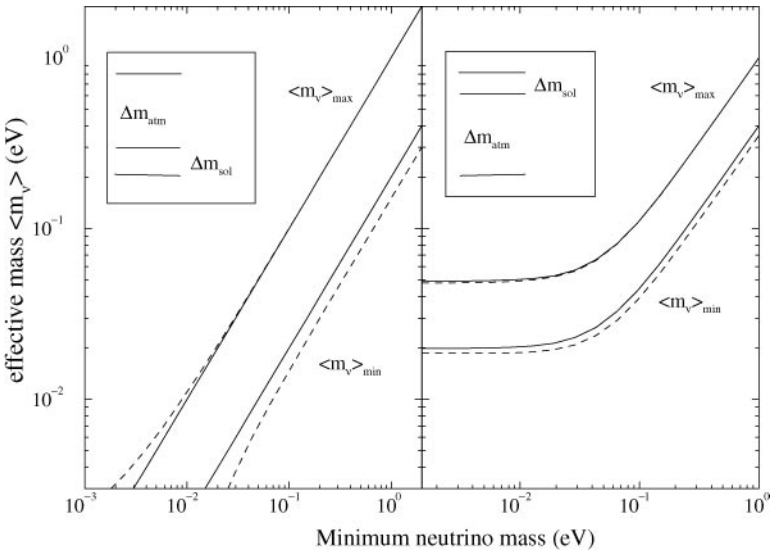

Figure 3 Effective mass $\langle m_\nu \rangle$ as a function of the smallest neutrino mass $m_{\min}$. The left panel is for the normal mass hierarchy, as indicated in the inset (not to scale), and the right panel is for the inverted hierarchy. Both panels are evaluated for the large-mixing-angle solar solution with $\Delta m^2_{\text{atm}} = 2.4 \times 10^{-3}$ eV^2, $\Delta m^2_{\text{sol}} = 4.5 \times 10^{-5}$ eV^2, and $|U_{e2}|^2 = 0.3$. The solid lines show $\langle m_\nu \rangle_{\max}$ and $\langle m_\nu \rangle_{\min}$, defined in Equation 21, for $U_{e3} = 0$; the dashed lines use the maximum value $|U_{e3}|^2 = 0.025$ allowed by the CHOOZ and PALO VERDE reactor experiments (12, 13).

Thus, if the search for $\beta\beta(0\nu)$ is successful and the value of $\langle m_\nu \rangle$ is determined, and at the same time the mixing angles $|U_{ei}|^2$ and the mass square differences Δm^2_{ij} are known from oscillation experiments, a range of absolute values of the neutrino masses can be deduced. This is illustrated in Figure 3, where we assume that $N = 3$, that the large-mixing-angle (LMA) solution of the solar neutrinos is correct, and that the atmospheric neutrino problem requires maximal mixing of the μ and τ neutrinos. We must consider two possibilities, the normal and inverted hierarchies (see insets in Figure 3), because from the given information we cannot distinguish between them. (Note that the uncertainty in the mixing parameters is not included in Figure 3.)

Naturally, if another constraint exists, for example a successful determination of the neutrino mass square $\sum_i |U_{ei}|^2 m_i^2$ in the tritium beta decay experiments, one can use the knowledge of $\langle m_\nu \rangle$ to determine or constrain the phases α_i.

Numerous analyses of the existing data correlate the current results of the neutrino oscillation searches, $\beta\beta(0\nu)$ experiments, tritium beta decay experiments, etc. We list here only a subset of the corresponding papers and apologize for omission of other work (see References 41–47).

One cannot predict, in general, the value of $\langle m_\nu \rangle$ using present knowledge. On the other hand, as shown in Figure 3 for the currently most likely oscillation scenario, one can show that certain classes of solutions, such as the inverted hierarchy, or the normal hierarchy with the smallest neutrino mass $\gg \sqrt{\Delta m^2_{\rm sol}}$ (degenerate neutrino spectrum), lead to potentially observable $\beta\beta(0\nu)$ decay.

2.4. $\beta\beta(0\nu)$ Decay and Other Lepton-Number-Violating Processes

The $\beta\beta(0\nu)$ decay is not the only possible observable manifestation of lepton number violation. Muon-positron conversion,

$$\mu^- + (A, Z) \rightarrow e^+ + (A, Z-2), \qquad 22.$$

and rare kaon decays $K_{\mu\mu\pi}$, $K_{ee\pi}$, and $K_{\mu e\pi}$,

$$K^+ \rightarrow \mu^+\mu^+\pi^-, \quad K^+ \rightarrow e^+e^+\pi^-, \quad K^+ \rightarrow \mu^+e^+\pi^-, \qquad 23.$$

are examples of processes where total lepton number conservation is violated and where good limits on the corresponding branching ratios exist (see Reference (48) for a more complete discussion). Like the $\beta\beta(0\nu)$ decay, these processes can be mediated by the exchange of a virtual massive Majorana neutrino. In that case, their rate is proportional to the quantity analogous to $\langle m_\nu \rangle$,

$$\langle m_{xy} \rangle \equiv \sum_i U_{xi} U_{yi} m_i, \qquad 24.$$

involving other lines of the neutrino mixing matrix U (in $\beta\beta(0\nu)$ the relevant quantity is $\langle m_{ee} \rangle$). Again, as in the $\beta\beta(0\nu)$ decay, other mechanisms are possible and might lead to faster rates.

Study of such decays, in principle, would allow one to constrain or determine the otherwise inaccessible Majorana phases in U. However, the present and foreseeable future of the experimental search has not reached the required sensitivity.

Considerable experimental effort has been devoted to the study of the $\mu^- \rightarrow e^+$ conversion. The best limit obtained to date is (49)

$$\frac{\Gamma(\mathrm{Ti} + \mu^- \rightarrow e^+ + \mathrm{Ca_{gs}})}{\Gamma(\mathrm{Ti} + \mu^- \rightarrow \nu_\mu + \mathrm{Sc})} < 1.7 \times 10^{-12}\ (90\%\ CL), \qquad 25.$$

and a substantial improvement is anticipated in proposed experiments. That branching ratio limit can be expressed as the limit on

$$\langle m_{\mu e} \rangle \equiv \left\langle \sum_i U_{ei} U_{\mu i} m_i \right\rangle < 17\,(82)\,\mathrm{MeV}, \qquad 26.$$

where the two limiting values reflect the dependence on the spin state (0 or 1) of the created proton pair.

Similarly, for the $K_{\mu\mu\pi}$ decay, the branching ratio is presently restricted to (see Reference (50) for a description of the limits on the other lepton-number-violating K decays)

$$\frac{\Gamma(K^+ \to \pi^- \mu^+ \mu^+)}{\Gamma(K^+ \to \text{all})} < 3.0 \times 10^{-9} \text{ (90\% CL)}. \quad 27.$$

Following Reference (51), this branching ratio limit can be expressed as the limit

$$\langle m_{\mu\mu} \rangle \equiv \sum_i U_{\mu i}^2 m_i < 4 \times 10^4 \text{ MeV}. \quad 28.$$

Since, obviously, $\langle m_{xy} \rangle \leq m_{\max}$, the present limits are far from constraining U for the three light neutrinos whose mass is restricted by the tritium beta decay experiments (52, 53) and the positive results of the atmospheric and solar neutrino oscillation experiments to be $\leq \mathcal{O}(\text{eV})$. The hypothetical subdominantly coupled heavy sterile neutrinos are also only marginally constrained (51).

Nevertheless, it is important to pursue searches for the $|\Delta L| = 2$ processes with $|\Delta L_\mu| \neq 0$, since they can generally yield nonvanishing results even when $\beta\beta(0\nu)$ decay is vanishing or very slow.

3. $\beta\beta(0\nu)$ MATRIX ELEMENTS

For all three modes of double beta decay ($\beta\beta(0\nu)$, $\beta\beta(2\nu)$, $\beta\beta(0\nu, \chi)$), one can separate, essentially without loss of accuracy, the phase space and nuclear parts of the rate formulae. All nuclear structure effects are then represented by the nuclear matrix elements. Reference (23) includes a rather complete list of references and the results of calculation of the nuclear matrix elements.

The half-life for the $\beta\beta(2\nu)$ decay mode can be written in the compact form, analogous to Equation 18 but without the factor $\langle m_\nu \rangle$,

$$\left[T_{1/2}^{2\nu}(0^+ \to 0^+)\right]^{-1} = G^{2\nu}(E_0, Z) \left| M_{\text{GT}}^{2\nu} \right|^2, \quad 29.$$

where again $G^{2\nu}$ is the exactly calculable phase-space integral containing all the relevant constants, and $M_{\text{GT}}^{2\nu}$ is the nuclear matrix element (there is no Fermi part, owing to the isospin conservation),

$$M_{\text{GT}}^{2\nu} = \sum_m \frac{\langle f || \sigma \tau_+ || m \rangle \langle m || \sigma \tau_+ || i \rangle}{E_m - (M_i + M_f)/2}, \quad 30.$$

where $|f\rangle (|i\rangle)$ are the 0^+ ground states of the final (initial) even-even nuclei of masses $M_f (M_i)$, and $|m\rangle$ are the 1^+ states in the intermediate odd-odd nucleus of energy E_m. The individual factors in Equation 30 have straightforward physical meaning; the last factor in the numerator is the amplitude of the β^- decay [or of the forward-angle (p, n) reaction] of the initial nucleus, and the first factor is the amplitude of the β^+ decay [or of the (n, p) reaction] of the final nucleus. Thus, the description of the $\beta\beta(2\nu)$ decay is equivalent to the description of the full beta strength functions of both the initial and final nuclei. The $\beta\beta(2\nu)$ rate is sensitive to details of nuclear structure, however, because the ground-state–to–ground-state transition exhausts only a very small fraction of the double GT sum

TABLE 1 Summary of experimentally measured $\beta\beta(2\nu)$ half-lives and matrix elements[a]

Isotope	$T^{2\nu}_{1/2}$ (y)	References	$M^{2\nu}_{GT}$ (MeV^{-1})
^{48}Ca	$(4.2 \pm 1.2) \times 10^{19}$	(55, 56)	0.05
^{76}Ge	$(1.3 \pm 0.1) \times 10^{21}$	(57–59)	0.15
^{82}Se	$(9.2 \pm 1.0) \times 10^{19}$	(60, 61)	0.10
$^{96}Zr^{\dagger}$	$(1.4^{+3.5}_{-0.5}) \times 10^{19}$	(62–64)	0.12
^{100}Mo	$(8.0 \pm 0.6) \times 10^{18}$	(65–70), (71)†	0.22
^{116}Cd	$(3.2 \pm 0.3) \times 10^{19}$	(72–74)	0.12
^{128}Te[b]	$(7.2 \pm 0.3) \times 10^{24}$	(75, 76)	0.025
^{130}Te[c]	$(2.7 \pm 0.1) \times 10^{21}$	(75)	0.017
^{136}Xe	$>8.1 \times 10^{20}$ (90% CL)	(77)	<0.03
$^{150}Nd^{\dagger}$	$7.0^{+11.8}_{-0.3} \times 10^{18}$	(68, 78)	0.07
^{238}U[d]	$(2.0 \pm 0.6) \times 10^{21}$	(79)	0.05

[a]See Section 4.3 for a discussion of the averaging procedure. In the "isotope" column, the symbol † indicates inconsistent results, in which case the uncertainty reflects the spread in the measured values. In the "references" column, the † indicates the outliers that were not used in the averaging. The nuclear matrix elements were deduced by using the phase-space factors of Reference (22) with the mean $T^{2\nu}_{1/2}$.

[b]Deduced from the geochemically determined half-life ratio $^{128}Te/^{130}Te$.

[c]Geochemical result includes all decay modes; other geochemical determinations only marginally agree.

[d]Radiochemical result, again for all decay modes.

rule (54). Description of the $\beta\beta(2\nu)$ thus represents a severe test of the nuclear models used in the evaluation of $M^{2\nu}_{GT}$. Table 1 lists the experimentally determined matrix elements for the $\beta\beta(2\nu)$ decay. Note that the nuclear structure effects cause variations by a factor of $\sim$10 in the matrix elements, i.e., by a factor of $\sim$100 in the half-lives.

The nuclear matrix elements defined in Equation 15 govern both $\beta\beta(0\nu)$ and $\beta\beta(0\nu, \chi)$ decay modes. However, the half-life of the $\beta\beta(0\nu, \chi)$ mode depends on the effective majoron-neutrino coupling constant $\langle g_{\nu\chi} \rangle$, instead of $\langle m_\nu \rangle$

$$\left[T^{0\nu,\chi}_{1/2}(0^+ \to 0^+)\right]^{-1} = G^{0\nu,\chi}(E_0, Z) \left| M^{0\nu}_{GT} - \frac{g_V^2}{g_A^2} M^{0\nu}_{F} \right|^2 \langle g_{\nu\chi} \rangle^2, \qquad 31.$$

where again $G^{0\nu,\chi}(E_0, Z)$ is the phase-space integral, tabulated, e.g., in Reference (21).

Throughout, we discuss only the $\beta\beta(0\nu)$ decay mediated by the exchange of a light massive Majorana neutrino and governed by the nuclear matrix elements (Equation 15). The rate of $\beta\beta(0\nu)$ mediated by other mechanisms, e.g., those that involve the right-handed current weak interactions, or the exchange of only heavy

particles (heavy neutrinos, supersymmetric particles, etc.), depends on other nuclear matrix elements. For a detailed discussion of their evaluation, see References (23, 24) and (36).

There are two basic approaches to the evaluation of the nuclear matrix elements for both the $\beta\beta(2\nu)$ and $\beta\beta(0\nu)$ decays: the quasiparticle random phase approximation (QRPA) and the nuclear shell model (NSM). As pointed out above, the factors that contribute to the $\beta\beta(2\nu)$ matrix elements are related to other nuclear phenomena and thus are testable. This is not so—or at least testing is much more difficult—for the matrix elements of the $\beta\beta(0\nu)$ mode. It is therefore less clear how to reliably estimate the uncertainty involved in their evaluation.

The QRPA has been the most popular theoretical tool in the recent past, because it explained the suppression, relative to the sum rule (54), of $M^{2\nu}_{\rm GT}$, and it is easy to use. The main physics ingredients of the method, relevant particularly for the testable $\beta\beta(2\nu)$ decay, are the repulsive particle-hole spin-isospin interaction and the attractive particle-particle interaction, which clearly play a decisive role in the concentration of the β^- strength in the giant GT resonance, and the relative suppression of the β^+ strength and its concentration at low excitation energies. Together, these two ingredients are able to explain the values of $M^{2\nu}_{\rm GT}$ provided the empirical parameter g_{pp}, the strength of the particle-particle interaction, is adjusted (but its adjusted value is, reassuringly, near its expected value). Yet, the QRPA is often criticized for two "undesirable" features. One is the sensitivity of $M^{2\nu}_{\rm GT}$ to the g_{pp} value, which decreases the predictive power of the method. The other is the fact that, for a realistic value of g_{pp}, the QRPA solutions are close to their critical value (so-called collapse, beyond which the solutions of the QRPA equations do not exist). The collapse indicates a phase transition, i.e., a rearrangement of the nuclear ground state. The QRPA is meant to describe small deviations from the unperturbed ground state and thus is not fully applicable near the point of collapse. Numerous attempts have been made to extend the method's range of validity, most of which involve corrections to the quasi-boson approximation (see, e.g., Reference 23).

Despite extensive work on this aspect of the QRPA, we do not know the effect of the more complicated configurations that are not included in the QRPA (which includes only the two-quasiparticle states and their iterations) on the double beta nuclear matrix elements, and in particular on the $\beta\beta(0\nu)$ ones. There is also a lack of detailed nuclear spectroscopy predictions (beyond the beta strength function).

The nuclear shell model (NSM), when computationally feasible, is the method of choice for the evaluation of double beta decay nuclear matrix elements. One chooses a set (limited basically by the capability of present-day computers) of valence single-particle states. Then one finds an effective Hamiltonian, usually based on the free nucleon-nucleon interaction but modified to describe the effective nucleon interaction for that particular set. All configurations (or at least a convergent set of them) are used in the diagonalization of the Hamiltonian and in the evaluation of the double beta decay nuclear matrix elements. The method is tested, and the Hamiltonian is adjusted, by requiring that it describe the spectroscopy (level energies and transition probabilities) of the relevant nuclei.

Despite the tremendous advances of the computational techniques, only a limited set of single-particle states can be included in the NSM. The effects of single-particle states that are excluded is usually simulated in the NSM by using effective operators, or more simply by using effective charges. Unfortunately, it is not clear what effective charges, if any (or indeed what effective operators), should be used in the NSM evaluation of the $\beta\beta(0\nu)$ matrix elements $M_{\rm F}^{0\nu}$ and $M_{\rm GT}^{0\nu}$, and it is not clear what related phenomena one can use to determine them.

Thus, each approach, QRPA and NSM, has its strengths and weaknesses, and naturally its critics and defenders. It is customary, although not really justified, to consider the spread of the theoretically calculated $\beta\beta(0\nu)$ nuclear matrix elements as a measure of their uncertainty. Clearly, a breakthrough in the evaluation of these matrix elements, or at least in the estimate of their uncertainty, would be very welcome. Given the experimental effort described in the following sections and the importance of the problem, we hope that a comparable theoretical effort will emerge and radically improve nuclear matrix element evaluation.

To emphasize the difficulty of evaluating the $\beta\beta(0\nu)$ nuclear matrix elements, let us stress once more that the presence of the neutrino propagator leads to the appearance of the "neutrino potential" $H(r, \bar{A})$, Equation 14. Then,

$$M_{\rm GT}^{0\nu} = \langle f | \sum_{lk} \vec{\sigma}_l \cdot \vec{\sigma}_k \tau_l^+ \tau_k^+ H(r_{lk}, \bar{A}) | i \rangle, \qquad 32.$$

$$M_{\rm F}^{0\nu} = \langle f | \sum_{lk} \tau_l^+ \tau_k^+ H(r_{lk}, \bar{A}) | i \rangle. \qquad 33.$$

Here the l, k summation is over all pairs of neutrons (or protons). Note that, owing to the presence of $H(r, \bar{A})$, the Fermi matrix element $M_{\rm F}^{0\nu}$ is nonvanishing even if isospin is conserved.

One can now expand the potential $H(r, \bar{A})$ in multipoles that correspond to the various angular momenta of the intermediate odd-odd nucleus. One finds, as expected from the high excitation energy (or high value of the momentum q of the virtual neutrino), that many multipoles give comparable contributions. Moreover, the 1^+ multipole, which is the only one that contributes to the $\beta\beta(2\nu)$ decay, is suppressed and contributes very little. Thus, a correct reproduction of measured $M_{\rm GT}^{2\nu}$ is a necessary but insufficient condition for equally successful evaluation of the $M_{\rm GT}^{0\nu}$ and $M_{\rm F}^{0\nu}$ nuclear matrix elements.

It has been often argued that, unlike $M_{\rm GT}^{2\nu}$, there is no suppression in $M_{\rm GT}^{0\nu}$ and $M_{\rm F}^{0\nu}$, and hence their values are less sensitive to nuclear structure details. This argument is based on the multipole decomposition, discussed above, in the various angular momenta and parities of the virtual states in the intermediate odd-odd nucleus. It turns out that the contributions of most of the mutipoles have the same sign and hence do not interfere with each other.

However, it is possible to expand the corresponding expression in an equivalent representation in terms of the angular momenta and parities of the pair of neutrons that are transformed into the pairs of protons. In this equally valid representation,

TABLE 2 $\beta\beta(0\nu)$ half-lives in units of 10^{26} y corresponding to $\langle m_\nu \rangle = 50$ meV for nuclear matrix elements evaluated in the references indicated

	References					
Nucleus	**(20)**	**(80)**	**(81)**	**(82)**	**(24, 83)**	**(84)**
^{48}Ca	12.7	35.3	—	—	—	10.0
^{76}Ge	6.8	70.8	56.0	9.3	12.8	14.4
^{82}Se	2.3	9.6	22.4	2.4	3.2	6.0
^{100}Mo	—	—	4.0	5.1	1.2	15.6
^{116}Cd	—	—	—	1.9	3.1	18.8
^{130}Te	0.6	23.2	2.8	2.0	3.6	3.4
^{136}Xe	—	48.4	13.2	8.8	21.2	7.2
^{150}Nd[a]	—	—	—	0.1	0.2	—
^{160}Gd[a]	—	—	—	3.4	—	—

[a]deformed nucleus; deformation not taken into account.

the dominant contribution of the $J = 0^+$ pairs is to a large extent cancelled by the contribution of all other, $J \neq 0^+$, pairs, which have an opposite sign. Thus, also in the $\beta\beta(0\nu)$ case the nuclear matrix elements depend on the small, and presumably poorly determined, pieces of the nuclear wave function.

Despite our reservations, in Table 2 we compare the $\beta\beta(0\nu)$ half-lives evaluated for $\langle m_\nu \rangle = 50$ meV with nuclear matrix elements evaluated in the cited references, chosen to represent the vast literature on the subject. The spread of the calculated values for the given parent nucleus gives some indication of the role played by the nuclear matrix elements. On the other hand, the spread of half-lives along the columns in Table 2 reflects the effects of both the phase space and the nuclear matrix elements. The methods used to evaluate them are the truncated shell model (20), NSM (80), QRPA with the schematic δ force interaction ($\alpha_1' = 390$ MeV fm^3, recalculated for $g_A = 1.25$) (81), QRPA with G-matrix based interaction (82), renormalized QRPA (24, 83), and QRPA without the p-n pairing (84). The calculated half-life uncertainty of about an order of magnitude, corresponding to a factor of $\sim$3 in $\langle m_\nu \rangle$, is apparent.

4. $\beta\beta(0\nu)$ EXPERIMENTAL OVERVIEW AND PAST $\beta\beta(0\nu)$ EXPERIMENTS

The various detection schemes for double beta decay are outlined elsewhere (1), so we merely mention the salient points here. Over the past 15 years, background reduction has allowed a large number of $\beta\beta(2\nu)$ half-life measurements. With this success behind us, the community is currently focusing on the more exciting goal of $\beta\beta(0\nu)$. The various modes of double beta decay are separated by the differences

in their electron sum energy spectrum, and—because $\beta\beta(0\nu)$ is identified by its distinguishing sum-energy peak—direct counting experiments with sufficient energy resolution are the focus of today's researchers. In most of these experiments, the source also serves as the detector.

Geochemical and radiochemical experiments, a mainstay of double beta decay physics through the 1970s and 1980s, do not distinguish the different modes. Thus, there is little interest in pursuing these techniques further. Instead, relatively new technologies such as bolometers and scintillating crystals are receiving attention. Tracking and foil-scintillator sandwich experiments are also being pursued, although the source and detector are separate. Amazingly, the old workhorse, the germanium detector, dominates the present $\beta\beta(0\nu)$ decay results and offers some of the most promising future proposals.

The study of double beta decay is about suppressing backgrounds. Therefore, in this section, we summarize the criteria for a good double beta decay experiment and then discuss the background issues in general. Finally, we describe past and current experiments.

4.1. Experimental Criteria

For the best sensitivity to $\langle m_\nu \rangle$, a detector must maximize the $\beta\beta(0\nu)$ count rate while minimizing the background. The signal sensitivity is approximately determined by the statistical precision (i.e., square root) of the background determination. Because the number of background counts increases linearly with time, the decay rate sensitivity scales as the square root of time. In turn, the $\langle m_\nu \rangle$ sensitivity scales as the square root of the decay rate, and therefore as the fourth root of the counting time. In an experiment with zero background, on the other hand, the $\langle m_\nu \rangle$ limit scales more quickly as the square root of the counting time. Explicitly, the limit on $\langle m_\nu \rangle$ can be expressed in terms of experimental parameters as (85)

$$\langle m_\nu \rangle = (2.50 \times 10^{-8}\,\mathrm{eV}) \left[\frac{W}{f x \epsilon G^{0\nu} |M^{0\nu}|^2} \right]^{1/2} \left[\frac{b \Delta E}{MT} \right]^{1/4} \text{background limited}$$

$$\langle m_\nu \rangle = (2.67 \times 10^{-8}\,\mathrm{eV}) \left[\frac{W}{f x \epsilon G^{0\nu} |M^{0\nu}|^2} \right]^{1/2} \times \frac{1}{\sqrt{MT}} \text{zero background}, \qquad 34.$$

where W is the molecular weight of the source material, f is the isotopic abundance, x is the number of double beta decay candidate atoms per molecule, ϵ is the detector efficiency, b is the number of background counts per kg · year · keV, ΔE is the energy window for $\beta\beta(0\nu)$ in keV, M is the mass of isotope in kilograms, T is the live time of the experiment in years, and $|M^{0\nu}|$ is shorthand for the $\beta\beta(0\nu)$ matrix elements given by Equation 18. Some of the criteria for optimizing the design of a $\beta\beta(0\nu)$ decay experiment are obvious whereas others are more subtle. It is clear from Equation 34 that one needs a large source mass. To reach the 50 meV region of interest indicated by the oscillation results, approximately a ton of isotope will be required. Another obvious requirement is a detector that is reliable and preferably easy to operate. Because the experiments are usually conducted in

remote underground laboratories, it is a great convenience if the experiment needs minimal maintenance.

The search for $\beta\beta(0\nu)$ decay is a search for a peak superimposed on a continuum. Therefore, good energy resolution is a must. Not only does good resolution improve the signal-to-background ratio in the peak search, but poor resolution smears the $\beta\beta(2\nu)$ tail up into the peak region to become a background itself.

Natural radioactivity is present in all materials at some level. The source and detector must be very low in such impurities. Furthermore, the detector must be shielded from the environment and its associated radioactivity. This shielding must also be radiopure. Because the total radioactivity of an impure material scales as its volume, it is usually an advantage to minimize the detector size. This can be most readily accomplished when the detector also serves as the source.

Cosmogenic activities build up in materials through nuclear reactions of cosmic-ray muons and their secondary products, especially neutrons. These can be a significant background contribution both for the source and for the shielding material. Some materials have no long-lived isotopes and thus have a built-in safeguard against cosmogenics. For experiments that must fight this problem, fabricating the apparatus underground and storing materials underground can greatly reduce this background. Unlike solid sources, a gaseous or liquid source can be continuously purified of such impurities.

Choosing an isotope with a large Q-value and matrix element improves the $\langle m_\nu \rangle$ sensitivity for a given measured half-life. But the nuclear theory of some isotopes is better understood than others. Because the only feasible experiment sensitive to $\langle m_\nu \rangle$ is double beta decay and because the half-life for this process depends on both parameters (Equation 18), it is advantageous to use a source isotope for which there is confidence in the theoretical calculations. Also, some nuclei, ^{100}Mo for example, have relatively fast $\beta\beta(2\nu)$ rates with respect to the theoretically anticipated $\beta\beta(0\nu)$ rate for a given $\langle m_\nu \rangle$. Because $\beta\beta(2\nu)$ is a potential background, the source choice may be important for detectors with modest or marginal energy resolution.

Radiochemical and geochemical experiments operate by detecting the daughter of the decay. However, since these techniques integrate over an exposure time, they cannot identify the mode of decay. But if an experiment could identify the daughter in coincidence with a real-time measurement of the decay energy, it would have a powerful tool for rejecting many backgrounds. In this case, only $\beta\beta(2\nu)$ would be a background. There are several possibilities for detecting the daughter. If the decay is to an excited state, one might be able to observe gamma rays that identify the daughter. Double beta candidates are initially in 0^+ states, and in many cases, transitions to excited 2^+ or 0^+ states are possible. However, the Q-value for these excited-state transitions is much smaller than for the ground-state transition, and therefore the decay rate for a given $\langle m_\nu \rangle$ value is much lower. For the 2^+ case, the matrix elements are also much smaller owing to the forbidden nature of the transition. One interesting possibility is offered by ^{150}Nd, where the excited state is relatively low in energy. But this excited state decays via internal conversion, requiring the detection of a 30 keV x ray to observe

the daughter. The most enticing situation, however, is that of the Xe-Ba system. The optical detection of the Ba daughter ion might be possible (as discussed in Section 5).

4.2. Backgrounds

Any extraneous energy deposit in the detector near the $\beta\beta(0\nu)$ Q-value limits the sensitivity to $\langle m_\nu \rangle$. Thus, any radioactive isotope with a Q-value greater than the $\beta\beta(0\nu)$ endpoint may be a potential background. Because the number of radioactive isotopes decreases with increasing Q, it is desirable to select a double beta decay candidate with as large a Q-value as possible. Beta- and alpha-emitting decays are easy to shield and thus are a problem only if they occur within the detector or on its surface. Penetrating gamma rays pose a more difficult problem. In this subsection, we consider the origin of various sources of background and some techniques for their mitigation.

4.2.1. NATURAL ACTIVITY The naturally occurring isotopes of U and Th and their daughters are present as impurities in all materials. The half-life of the chain patriarch is comparable to the age of the universe but very short compared to the half-life sensitivity of the $\beta\beta(0\nu)$ experiments. Therefore, even a small quantity of U or Th will create a significant background. In particular, ^{214}Bi and ^{208}Tl have large Q-values, and the decay spectra will overlap the endpoint of almost all the $\beta\beta(0\nu)$ candidates. Even tracking experiments have difficulty with these two isotopes because of their beta decays, which are followed promptly by internal conversion, resulting in a two-electron event that mimics $\beta\beta(0\nu)$ or $\beta\beta(2\nu)$. Careful selection of materials and purification have been successful, if difficult, solutions to these problems. In the past decade, great strides have been made in purifying some materials. Of particular note are liquid scintillator (86), electroformed Cu (87), and CVD (chemical vapor deposited) nickel (88). The radioactive chains may or may not be in equilibrium, depending on the sample's history, because chemical treatment or purification can disproportionately eliminate the daughters.

Radon gas, either ^{222}Rn or ^{220}Rn, is especially intrusive and may infiltrate a detector's sensitive region. These parents to ^{214}Bi and ^{208}Tl are mobile and diffuse through many materials. Their daughters tend to be charged and stick to dust or any other electrostatic surface. Many experiments eliminate Rn from the detector vicinity by purging the volume immediately surrounding it with N_2 gas that has boiled off from a liquid nitrogen (LN) supply. Because Rn freezes out at LN temperatures, the boil-off gas tends to be very low in Rn, especially compared with the laboratory air being displaced. Some groups have also installed charcoal Rn scrubbers into the laboratory airstream.

Activities such as ^{3}H, ^{14}C, and ^{40}K are also naturally present but their Q-values are too low to interfere with $\beta\beta(0\nu)$ experiments. However, many $\beta\beta(0\nu)$ experiments double as dark matter experiments by studying the low end of their energy spectrum for possible elastic scattering of WIMPS (weakly interacting

massive particles). These experiments have to consider a larger pool of potential background isotopes.

4.2.2. COSMOGENIC AND INDUCED ACTIVITIES Long-lived radioactive isotopes can be produced through various nuclear reactions. Many of these isotopes can have decay energies that exceed the $\beta\beta(0\nu)$ Q-value and thus can create a background. Such activities can be produced in the detector or the shielding material. In particular, long-lived isotopes of the source element can be very difficult to remove by purification. The troublesome ^{68}Ge 271-day activity that builds up in Ge detectors is a good example of this problem. Short-lived activities can also create background if created in situ while the experiment is operating. In this section, we discuss several nuclear processes that should be considered. The magnitude of the background due to each process is material-dependent, and the flux of the projectiles that induce the activities depends on the environment. In fact, many processes are greatly minimized by going underground, where the cosmic-ray flux is decreased.

Neutron capture produces gamma rays and frequently a radioactive isotope. Because neutrons are neutral and difficult to identify with anticoincidence detectors, they can be a significant problem. On the Earth's surface, most neutrons arise from the cosmic-ray hadronic component. In shallow underground laboratories, secondary neutrons from cosmic-ray muon interactions can form a large contribution to the total neutron flux. In deep sites, however, the neutron flux is dominated by (α, n) reactions and fission neutrons from the laboratory's rock walls. Siting the laboratory deep underground, covering the walls with shielding material to reduce the overall flux inside the laboratory, and placing neutron shielding around the detector can help control this background.

Fast-neutron reactions also need consideration. ^{68}Ge, for example, is produced by fast-neutron (>100 MeV) interactions on stable Ge isotopes. Above ground, the dominant source of these fast neutrons are secondaries produced by cosmic rays. Once the material is taken deep underground, the problem is mitigated for the most part, as only the residual surface production remains. But estimating the underground production rate at a given depth requires neutron flux data. Several integral measurements of the neutron flux underground are available, along with estimates of the neutron production due to muons. However, since the neutron flux falls very quickly with energy, it is difficult to deduce the higher energy flux from these measurements. A summary of the past measurements and a calculation of the fast neutron flux is given in Reference (89), and a program to measure the flux is being developed (90).

Muons and muon-induced electromagnetic showers can produce background also. Going deep underground reduces the flux, and veto systems surrounding the detector eliminate any prompt activity observed in coincidence. However, inelastic muon scattering and μ^- capture produce delayed events inside the detector after the muon signal. If this time delay is too long or if the muon flux is too high, anticoincidence techniques are insufficient. Additional depth can remedy this problem. For high-Z materials, μ^- capture dominates over muon decay (91)

and the neutron multiplicity is of order 1, with an energy spectrum extending to many tens of MeV (92). Many of the solar neutrino, dark matter, and double beta decay experiments have analyzed the possible spallation products that might be produced (see, e.g., Reference (93), which gives a brief general discussion of the topic).

4.2.3. ARTIFICIALLY PRODUCED ACTIVITY Artificial radioactive isotopes can also be present in materials. For example, $\approx 10^{15}$ Bq of ^{239,240}Pu from the above-ground testing of nuclear weapons coats the surface of the Earth. Nuclear accidents such as that at Chernobyl have introduced long-lived isotopes, e.g., ^{137}Cs, ^{90}Sr, and Pu into the environment. When considering what backgrounds might be present, it is prudent to consider these exotic possibilities. Xe double beta experiments must take into account the noble gas radioactive isotopes ^{42}Ar and ^{85}Kr, which arise from the venting of reactors and atmospheric testing.

4.2.4. $\beta\beta(2\nu)$ AS A BACKGROUND When searching for the $\beta\beta(0\nu)$ peak, one must consider $\beta\beta(2\nu)$ decay as a potential ultimate background. Near the endpoint energy (Q), the $\beta\beta(2\nu)$ spectrum has very little strength. But since $T^{2\nu}_{1/2}$ is much shorter than $T^{0\nu}_{1/2}$, the effect of resolution (shown in Figure 1) must be considered. Roughly speaking, the $\beta\beta(2\nu)$ counts within one peak width (ΔE) centered on Q will contribute to the $\beta\beta(0\nu)$ peak region and be a background. The fraction F of the $\beta\beta(2\nu)$ counts in the peak region can be approximated by

$$F = \frac{7Q\delta^6}{m_e}, \qquad 35.$$

where $\delta = \Delta E/Q$ is the FWHM energy resolution expressed as a fraction and m_e is the electron mass. The coefficient 7 is for a resolution of 5%. This coefficient depends moderately on resolution and is 8.5 at 1% and 5 at 10%. An expression for the $\beta\beta(0\nu)$ signal (S) to $\beta\beta(2\nu)$ background (B) ratio can then be written as

$$\frac{S}{B} = \frac{m_e}{7Q\delta^6}\frac{\Gamma_{0\nu}}{\Gamma_{2\nu}} = \frac{m_e}{7Q\delta^6}\frac{T^{2\nu}_{1/2}}{T^{0\nu}_{1/2}}. \qquad 36.$$

Although this approximation cannot replace a Monte Carlo simulation of an experiment's performance, it clearly indicates that good energy resolution is critical. But, in addition, the ratio of $T^{0\nu}_{1/2}$ (for $\langle m_\nu \rangle = 1$ eV) to $T^{2\nu}_{1/2}$ can vary from 5000 to 100,000 depending on the isotope's Q-value and matrix element estimate. Therefore, the choice of isotope merits consideration.

For a S/B of 1, the $\langle m_\nu \rangle$ sensitivity limit due to the $\beta\beta(2\nu)$ background can be estimated as

$$\langle m_\nu \rangle^2 \sim \frac{7Q\delta^6}{m_e}\frac{G_{2\nu}}{G_{0\nu}}\frac{|M^{2\nu}|^2}{|M^{0\nu}|^2}. \qquad 37.$$

Note that using an asymmetric 0ν window defined by $Q < E < Q + \Delta E/2$ reduces S by a factor of 2 but decreases B by a factor of ≈ 16. This is exploited by some

experiments where the resolution is not ideal. A previous calculation of the $\beta\beta(2\nu)$ contribution to the upper half of the $\beta\beta(0\nu)$ window differs from this estimate; Moe (94) agrees with the present result.

4.3. Past Experiments

This section is meant to embellish the work of Reference (1), not replace it. Thus, we de-emphasize material already covered there. The impressive progress in systematically cataloging $\beta\beta(2\nu)$ rates is detailed in Reference (28) and summarized in Table 1, which lists average values of the 10 measured $\beta\beta(2\nu)$ half-lives and the $|M^{2\nu}|$ values deduced from them. The quoted value for each parent nucleus is the weighted average of the chosen measurements. The average includes selected measurements with quoted uncertainties small enough to significantly affect the average. To assign the individual uncertainty associated with each measurement, we first separately averaged the asymmetric statistical and systematic errors and then added the two classes of errors in quadrature. The summarized $T^{2\nu}_{1/2}$ are quoted at the 68% confidence level. In the individual measurements where the uncertainty range was quoted at a different confidence level, we scaled the uncertainties to correspond to 68% confidence level. In the case of ^{96}Zr, the measurements are inconsistent and we chose the spread of the measurements as an indication of the uncertainty in the measured $T^{2\nu}_{1/2}$. In the case of ^{100}Mo, one measurement was very different from the others and we excluded it from the average. The nuclear matrix elements were deduced by using the phase-space factors of Reference (22). This procedure is somewhat arbitrary, but the details on the half-life measurements can be found in the cited references. The $T^{2\nu}_{1/2}$ of ^{136}Xe, not yet measured, is of interest because this isotope is under consideration for major upcoming experiments. We list its limit in the table.

In one case, namely the double beta decay of ^{100}Mo, the transition to the excited 0^+ state at 1.13 MeV in ^{100}Ru has been observed (95, 96). That state de-excites by emission of two gamma rays; their observation serves as a convenient and clean signature of the decay. The resulting averaged half-life, $T_{1/2} = (6.8 \pm 1.2) \times 10^{20}$ y, corresponds to a matrix element of similar magnitude as the 2ν transition to the ^{100}Ru ground state, in agreement with expectations (97). Similar transitions are possible in other double beta decay candidates but have not yet been observed.

The $\beta\beta(0\nu)$ half-life limits have also improved for many isotopes and are summarized in Table 3. The spread of calculated $T^{0\nu}_{1/2}$ given in Table 2 illustrates the uncertainty in $\langle m_\nu \rangle$ due to the uncertainty in the nuclear physics. As mentioned above, the spread in the half-lives is about an order of magnitude and thus the spread in deduced $\langle m_\nu \rangle$ would be about a factor of 3. The best limits come from the ^{76}Ge experiments, which indicate that $\langle m_\nu \rangle < 0.3$–1 eV.

The half-life limits for the majoron mode are also improving. Like the $\beta\beta(2\nu)$ mode, the $\beta\beta(0\nu, \chi)$ spectrum is a continuum, and therefore the limits, summarized in Table 4, are more comparable to $\beta\beta(2\nu)$ than to $\beta\beta(0\nu)$. We have considered only majoron decay modes that emit a single majoron and list in Table 4 the half-life limits and the corresponding $\langle g_{\nu,\chi} \rangle$ values. (See Equation 31 for the relationship

TABLE 3 Best reported limits[a] on $T^{0\nu}_{1/2}$

Isotope	$T^{0\nu}_{1/2}$ (y)	$\langle m_\nu \rangle$ (eV)	Reference
^{48}Ca	$>9.5 \times 10^{21}$ (76%)	<8.3	(98)
^{76}Ge	$>1.9 \times 10^{25}$	<0.35	(57)
	$>1.6 \times 10^{25}$	<0.33–1.35	(99)
^{82}Se	$>2.7 \times 10^{22}$ (68%)	<5	(60)
^{100}Mo	$>5.5 \times 10^{22}$	<2.1	(100)
^{116}Cd	$>7 \times 10^{22}$	<2.6	(73)
^{128,130}Te	$\frac{T_{1/2}(130)}{T_{1/2}(128)} = (3.52 \pm 0.11) \times 10^{-4}$ (geochemical)	<1.1–1.5	(75)
^{128}Te	$>7.7 \times 10^{24}$	<1.1–1.5	(75)
^{130}Te	$>1.4 \times 10^{23}$	<1.1–2.6	(101)
^{136}Xe	$>4.4 \times 10^{23}$	<1.8–5.2	(102)
^{150}Nd	$>1.2 \times 10^{21}$	<3	(68)

[a]The $\langle m_\nu \rangle$ limits and ranges are those deduced by the authors using their choices of matrix elements in the experimental papers cited. All are quoted at the 90% confidence level except as noted. The range of matrix elements that relate $T^{0\nu}_{1/2}$ to $\langle m_\nu \rangle$ can be found in Table 2.

TABLE 4 The most restrictive $\beta\beta(0\nu, \chi)$ limits[a]

Isotope	$T^{0\nu,\chi}_{1/2}$ (y)	$\langle g_{\nu,\chi} \rangle$	Reference
^{48}Ca	$>7.2 \times 10^{20}$	$<5.3 \times 10^{-4}$	(103)
^{76}Ge	$>6.4 \times 10^{22}$	$<8.1 \times 10^{-5}$	(57)
^{82}Se	$>2.4 \times 10^{21}$	$<(2.3–4.3) \times 10^{-4}$	(61)
^{96}Zr	$>3.5 \times 10^{20}$	$<(2.6–4.9) \times 10^{-4}$	(62)
^{100}Mo	$>5.4 \times 10^{21}$ (68%)	$<7.3 \times 10^{-5}$	(100)
^{116}Cd	$>3.7 \times 10^{21}$	$<1.2 \times 10^{-4}$	(73)
^{128}Te	$>7.7 \times 10^{24}$ (geochemical)	$<3 \times 10^{-5}$	(75)
^{130}Te	$>1.4 \times 10^{21}$	$<(2.6–6.7) \times 10^{-4}$	(101)
^{136}Xe	$>7.2 \times 10^{21}$	$<(1.3–3.8) \times 10^{-4}$	(102)
^{150}Nd	$>2.8 \times 10^{20}$	$<1 \times 10^{-4}$	(68)

[a]The $\langle g_{\nu,\chi} \rangle$ limits are those deduced by the authors of the experimental papers cited. All are quoted at the 90% confidence level except as noted. The total geochemical measured decay rate of ^{128}Te is used as its $\beta\beta(0\nu, \chi)$ limit. The range of matrix elements that relate $T^{0\nu\,\chi}_{1/2}$ to $\langle g_{\nu,\chi} \rangle$ can be deduced from the entries in Table 2.

between $T_{1/2}^{0\nu,\chi}$ and $\langle g_{\nu,\chi}\rangle$.) Note that, naturally, the deduced $\langle g_{\nu,\chi}\rangle$ limits depend on the nuclear matrix elements.

Interestingly, the best constraint on $\langle g_{\nu,\chi}\rangle$ comes from ^{128}Te, which has the longest measured total half-life. Furthermore, its Q-value is very low, resulting in a relative enhancement of the phase-space factors for the $\beta\beta(0\nu,\ \chi)$ and $\beta\beta(0\nu)$ modes compared with the $\beta\beta(2\nu)$ mode. Therefore, even though the observed rate is probably due to the $\beta\beta(2\nu)$ decay, a conservative assumption is to assign all the rate to an exotic mode when estimating parameter limits. In the case of ^{128}Te, the limit on $\langle g_{\nu,\chi}\rangle$ of $\leq 10^{-5}$ is the best, and for $\beta\beta(0\nu)$ the limit of $\approx$1 eV is competitive.

In the remainder of this section, we discuss selected recent double beta decay experiments that can be considered effective prototypes for future programs. We have ordered the discussion in the current section according to experimental technique to parallel Section 5.

4.3.1. MIBETA The MIBETA experiment (101) used TeO_2 crystals as bolometers. These detectors exploit the low heat capacity of the crystals at low temperature. A small energy deposit therefore results in a significant temperature increase of the crystal. The experiment consisted of an array of 20 crystals totaling 6.8 kg. Because ^{130}Te is 33.8% naturally abundant, enrichment was not necessary, although two crystals were enriched to 93% in ^{130}Te and two others were enriched to 95% in ^{128}Te. The crystals were arranged into a tower of five layers of four detectors within a dilution refrigerator 3500 mwe underground at the Laboratori Nazionali del Gran Sasso. The tower frame was made of oxygen-free high-conductivity (OFHC) copper and the crystal supports of Teflon. The temperature sensors were neutron-transmutation-doped germanium thermistors. Old Roman lead ($<$4 mBq/kg ^{210}Pb) was placed inside the cryostat surrounding the tower. The dilution refrigerator itself was shielded with low-activity lead (16 ± 4 Bq/kg ^{210}Pb). The array was operated at a temperature of $\approx$12 mK with an array-averaged resolution of $\approx$8 keV FWHM (0.3%) at the $\beta\beta(0\nu)$ endpoint energy of 2.529 MeV. Because thermal detectors are sensitive over their entire volume, they are susceptible to surface contamination, and indeed these crystals did observe a surface alpha activity that contributed significantly to the $\beta\beta(0\nu)$ window. The cosmogenically produced activities in Te are short-lived and therefore posed no significant problem.

4.3.2. GOTTHARD TUNNEL The Gotthard Xe experiment (102) used a five-atm gas time projection chamber with 3.3 kg of 62.5% enriched ^{136}Xe. The tracking feature of the detector permitted the identification of two-electron tracks indicative of double beta decay. The energy resolution at the $\beta\beta(0\nu)$ endpoint (2.481 MeV) was $\approx$165 keV FWHM (6.6%). The dominant background for $\beta\beta(0\nu)$ was concluded to be Compton-scattered electrons from natural gamma activities. These electrons were occasionally misidentified as two-electron events. Cosmogenic activities are not a serious issue for Xe experiments because there are no long-lived Xe isotopes and liquid or gaseous Xe can be continuously purged of non-Xe isotopes.

4.3.3. HEIDELBERG-MOSCOW AND IGEX The Heidelberg-Moscow (HM) (57, 104) and International Germanium Experiment (IGEX) (99) collaborations both used Ge detectors 86% enriched in ^{76}Ge. HM used 125.5 moles of active material whereas IGEX used 90 moles. With comparable masses and run times, the results from the two experiments are similar; HM posted a modestly better $T^{0\nu}_{1/2}$ limit. Because $\beta\beta(0\nu)$ events produce localized ionization in the detectors and many backgrounds (e.g., Compton scattering of gamma rays) produce multisite energy deposits, both experiments used pulse-shape discrimination to reduce background.

HM identifies the radioactivities that contribute to the data by their associated peaks within the spectrum. With these identifications, the response of the detectors to these radioactivities was simulated with Monte Carlo. A fit to the actual data using the Monte Carlo spectra indicated the location of the activity. The conclusion of that work (57) is that the copper parts of the cryostat contained the majority of the background sources.

IGEX measured the cosmogenic activity produced in Ge crystals and compared that to a calculation of the expected rate based on the measured surface neutron flux and neutron interaction cross sections (105). The calculated rates and measured rates agreed well. The IGEX group found that initially ^{68}Ge was the dominant cosmogenic activity, with the longer-lived ^{60}Co dominating at later times. The rate of ^{68}Ge can be determined within each crystal by measuring the intensity of the 10.4 keV x-ray peak. The count rate in the $\beta\beta(0\nu)$ window could be mostly attributed to radon intrusion. However, the authors concluded that if Rn were reduced, Ge activation isotopes would be the limiting background source in the IGEX experiment.

The two experiments quote similar background levels in the $\beta\beta(0\nu)$ region of $\approx$0.20 counts/(keV $\cdot$ kg $\cdot$ y) before pulse shape discrimination and $\approx$0.06 counts/(keV $\cdot$ kg $\cdot$ y) after. However, remarkably, the two collaborations reach very different conclusions as to the composition of the limiting component of the background in these experiments. This is one of the most critical debates in experimental $\beta\beta(0\nu)$ research today, since the design of the next generation of Ge detector experiments depends heavily on its outcome (see Section 5.1).

During the preparation of this review (January 2002), Klapdor-Kleingrothaus et al. (106) used the HM data to claim evidence for $\beta\beta(0\nu)$ in ^{76}Ge with a $T^{0\nu}_{1/2} = (0.8\text{–}18.3) \times 10^{25}$ y. If true, this result is extremely important and hence requires extensive substantiation and review. However, by itself, the paper does not sufficiently support the claim (107). Its deficiencies do not necessarily mean that the claim is wrong, but they indicate that the assessment of this result by the double beta decay community will take time. In particular, the questions raised by Aalseth et al. (107) should be answered first by the authors of Reference (106).

4.3.4. UCI, ELEGANTS, AND NEMO The time projection chamber experiment (TPC) at the University of California at Irvine measured several isotopes. Each sample, a few tens of grams, was placed as a thin foil on the central electrode of a TPC. On either side of this source plane were drift regions for recording a three-dimensional image of the ionization trails produced by the $\beta\beta(2\nu)$ electrons. The experiment

successfully used the tracking capability to determine several kinematic parameters that characterized events. This information was critical to reducing backgrounds to a level that allowed the first direct detection of double beta decay (60, 108, 109). The drawback of the design is the limited amount of source mass compared with the size and complexity of the detector.

The best limits on ^{100}Mo $\beta\beta(0\nu)$ decay come from the ELEGANTS (ELEctron GAmma-ray Neutrino TeleScope) experiments (100). The emitted electrons in this experiment traversed drift chambers that measured their trajectories and then passed into plastic scintillator that measured their energies and arrival times. NaI arrays surrounded the apparatus to provide gamma- and x-ray observation. Copper and lead shielding enclosed the detectors. The 171 g ^{100}Mo source was two thin foils situated between the drift chambers. This detector had a diminished $\beta\beta(0\nu)$ detection efficiency compared with the Ge detectors or bolometers. However, it had additional background rejection power because of its measurement of several kinematic parameters. The dominant backgrounds in the $\beta\beta(0\nu)$ window were identified to be ^{214}Bi and ^{208}Tl contained in the source film and detector elements.

The NEMO-2 experiment (Neutrino Ettore Majorana Observatory) (61, 62, 65, 72, 110) analyzed the $\beta\beta(2\nu)$ rate for several isotopes. The detector had a tracking volume of 1 m^3 of He gas with two sides covered by scintillator calorimeters. The tracking volume was bisected by a thin source plane and consisted of frames containing crossed Geiger cells. An electron was defined by a track passing from the source foil to the calorimeter. Three-dimensional track measurements were made by using the drift times and plasma propagation times of the Geiger cells. The energy was determined with the calorimeters. The various source foils weighed up to about 175 g.

These tracking experiments all had small source masses, modest energy resolution, and a complex apparatus. As a result, it will be a challenge for future efforts modeled on these designs to be competitive in the search for $\beta\beta(0\nu)$ decay.

4.3.5. SCINTILLATING CRYSTALS There has been some progress in making large scintillating crystals that contain an appreciable amount of double beta decay isotope. The Bejing group used CaF_2 (98) to study ^{48}Ca and placed a lower limit on the $\beta\beta(0\nu)$ decay rate. A Kiev-Firenze collaboration (73) has used $^{116}CdWO_4$ scintillators to measure the $\beta\beta(2\nu)$ half-life of ^{116}Cd and placed limits on the $\beta\beta(0\nu)$ and $\beta\beta(0\nu, \chi)$ modes. Future experiments will exploit similar crystal technologies.

5. FUTURE $\beta\beta(0\nu)$ EXPERIMENTS AND PROPOSALS

5.1. The Various Proposals

The criteria described in Section 4 are frequently incompatible. Thus, no past or proposed experiment can optimize them all simultaneously. We are aware of 14 ideas or proposals for $\beta\beta(0\nu)$ experiments. Table 5 summarizes these proposals,

TABLE 5 Proposed or suggested future $\beta\beta(0\nu)$ experiments, grouped by the magnitude of the proposed isotope mass[a]

Experiment	Source	Detector description	Sensitivity to $T^{0\nu}_{1/2}$ (y)
COBRA (111)	^{130}Te	10 kg CdTe semiconductors	1×10^{24}
DCBA (112)	^{150}Nd	20 kg ^{enr}Nd layers between tracking chambers	2×10^{25}
NEMO-3 (113)	^{100}Mo	10 kg of $\beta\beta(0\nu)$ isotopes (7 kg Mo) with tracking	4×10^{24}
CAMEO (114)	^{116}Cd	1 t $CdWO_4$ crystals in liquid scintillator	$>10^{26}$
CANDLES (115)	^{48}Ca	several tons of CaF_2 crystals in liquid scintillator	1×10^{26}
CUORE (116)	^{130}Te	750 kg TeO_2 bolometers	2×10^{26}
EXO (73)	^{136}Xe	1 t ^{enr}Xe TPC (gas or liquid)	8×10^{26}
GEM (117)	^{76}Ge	1 t ^{enr}Ge diodes in liquid N	7×10^{27}
GENIUS (118)	^{76}Ge	1 t 86% ^{enr}Ge diodes in liquid N	1×10^{28}
GSO (119, 120)	^{160}Gd	2 t Gd_2SiO_5:Ce crystal scintillator in liquid scintillator	2×10^{26}
Majorana (121)	^{76}Ge	0.5 t 86% segmented ^{enr}Ge diodes	3×10^{27}
MOON (122)	^{100}Mo	34 t ^{nat}Mo sheets between plastic scintillator	1×10^{27}
Xe (123)	^{136}Xe	1.56 t of ^{enr}Xe in liquid scintillator	5×10^{26}
XMASS (124)	^{136}Xe	10 t of liquid Xe	3×10^{26}

[a]The $T^{0\nu}_{1/2}$ sensitivities are those estimated by the collaborators but scaled for five years of data taking. These anticipated limits should be used with caution, since they are based on assumptions about backgrounds for experiments that do not yet exist. Because some proposals are more conservative than others in their background estimates, one should not use this table to contrast the experiments. See Table 2 for the range of matrix elements that relate $T^{0\nu}_{1/2}$ to $\langle m_\nu \rangle$.

dividing them into two groups according to source mass and listing them alphabetically within each group. Each proposal chooses a different approach to attain this optimization. Five of them are substantially developed and have the potential to reach the crucial 50 meV region. Although we briefly mention all 14 proposals, we devote particular attention to these five: CUORE, EXO, GENIUS, Majorana, and MOON.

5.1.1. CUORE The success of the MIBETA experiment inspired the Cryogenic Underground Observatory for Rare Events (CUORE) proposal (125). One thousand TeO_2 crystals of 750 g each will be operated as a collection of bolometers. The detectors will be collected into 25 separate towers of 40 crystals. Each tower will have 10 planes of 4 crystals each. One such plane has already been successfully tested, and a single tower prototype called CUORICINO has been approved.

The energy resolution at the $\beta\beta(0\nu)$ peak (2.529 MeV) is expected to be about 5 keV FWHM ($\approx$0.2%). A low energy threshold of 5–10 keV is anticipated, so the experiment will also search for dark matter. The background has been measured in the first plane to be $\approx$0.5 counts/(keV · kg · y). However, a major component of this background is surface contamination arising from the use of cerium oxide polishing compound, which tends to be high in thorium. With this problem solved, the experimenters project a conservative estimate of the background to be $\approx$0.01 counts/(keV · kg · y).

A major advantage of this proposal is that the natural abundance of ^{130}Te is 34%. No enrichment is needed, resulting in significant cost savings. As with MIBETA, the cosmogenic activities within the TeO_2 crystals are not a serious concern. On the other hand, the crystal mounts and cryostat comprise a significant amount of material close to the bolometers. Much of the cryostat is shielded with Roman-period lead, but a fair quantity of copper and Teflon remain close to the crystals.

5.1.2. EXO The Enriched Xenon Observatory (EXO) (126) proposes to use up to 10 tons of 60–80% enriched ^{136}Xe. The unique aspect of this proposal is the plan to detect the ^{136}Ba daughter ion correlated with the decay. If the technique is perfected, it would eliminate all background except that associated with $\beta\beta(2\nu)$. The real-time optical detection of the daughter Ba ion, initially suggested in Reference (94), might be possible if the ion can be localized and probed with lasers. The spectroscopy has been used for Ba^+ ions in atom traps. However, the additional technology to detect single Ba ions in a condensed medium, or to extract single Ba ions from a condensed medium and trap them, must be demonstrated for this application. For optical detection, the alkali-like Ba^+ ion is excited from a $6^2S_{1/2}$ ground state to a $6^2P_{1/2}$ with a 493 nm laser. Because this excited state has a 30% branching ratio to a $5^4D_{3/2}$ metastable state, the ion is detected by re-exciting this metastable state to the 6P state using a 650 nm laser, and then observing the resulting decay back to the ground state. This procedure can be repeated millions of times per second on a single ion to produce a significant signal.

EXO is presently considering two detector concepts: high-pressure-gas Xe TPC or Liquid Xe (LXe) scintillator. The TPC baseline design consists of two 35 m^3 modules at $\approx$20 atm for a total of 8.4 t of Xe. The Xe would be contained in a nonstructural bag within a pressurized buffer gas to constrain the Xe to the active region. The spatial resolution and typical beta particle range (5 cm) will permit the identification of the high-ionization-density points at the terminus of the beta tracks, aiding in the separation of two-electron events from one-electron backgrounds such as Compton scatters. Upon a trigger of an event near the $\beta\beta(0\nu)$ peak energy, 2.481 MeV, the lasers are directed to the decay point to excite the Ba^+ ion. One complication is that the $\beta\beta(0\nu)$ of ^{136}Xe produces a Ba^{++} ion whereas the spectroscopy requires a Ba^+ ion. Because Xe is a tightly bound atom, charge exchange with the Ba ion is unlikely and a quenching gas is required to neutralize one stage of ionization.

The EXO LXe concept has the advantage of being much smaller than the TPC because of the high density of LXe. The scintillation readout has better energy

resolution but cannot spatially resolve the high-ionization points. The higher density makes the scattering of the laser light too great for optical detection of the Ba^+ in situ. However, once the Ba ion is localized via its scintillation and ionization, it might be extracted via a cold-finger electrode coated in frozen Xe (M. Vient, unpublished observation). The ion is electrostatically attracted to the cold finger, which later can be heated to evaporate the Xe and release the Ba ion into a radio-frequency quadrupole trap. At that point, the Ba^{++} captures an electron to become Ba^+, is laser cooled, and is optically detected. The efficiency of the tagging has yet to be demonstrated and is a focus of current research.

The collaboration is currently performing experiments to optimize the energy resolution for both configurations. The resolution is a critical parameter, since $\beta\beta(2\nu)$ would then be the lone background if the Ba tagging is successful. Tests to determine the viability of the Ba extraction process are also being performed. The EXO collaboration has received funding to proceed with a 100 kg enriched Xe detector without Ba tagging. This initial prototype will operate at the Waste Isolation Pilot Plant (WIPP) in southern New Mexico.

5.1.3. GENIUS The understanding of Ge detectors has been developed over more than 30 years of experience. The potential of these detectors lies in their great energy resolution, ease of operation, and the extensive body of experience relating to the reduction of backgrounds. This potential is not yet exhausted, as is evidenced by the GENIUS and Majorana proposals, which build on the experimenters' previous efforts.

The GENIUS (Germanium Nitrogen Underground Setup) (118) proposal evolved from the HM experiment. Driving the design of this proposed Ge detector array experiment is the evidence that the dominant background in the HM experiment was due to radioactivity external to the Ge. (The reader should contrast this with the motivation for the design of the Majorana proposal described below.) An array of 2.5 kg, p-type Ge crystals would be operated "naked" within a large liquid nitrogen (LN) bath. The use of naked crystals moves the external activity outside the LN region. P-type crystals have a dead layer on the external surface that reduces their sensitivity to external beta and alpha activity. Due to its low stopping power, roughly 12 m of LN is required to shield the crystals from the ambient gamma-ray flux at the intended experimental site at Gran Sasso. By immersion in LN, the optimal operating temperature is maintained without a bulky cryostat, and a test of the naked operation of a crystal in a 50 l dewar has been successful (127). The results indicate that the performance of the detector was comparable to those operated in a conventional vacuum-tight cryostat system. The measurements also indicate that very little cross talk occurs between naked detectors and that an extended distance ($\approx$6 m) between the FET and the crystal does not degrade the signal.

The proposal anticipates an energy resolution of $\approx$6 keV FWHM (0.3%) and a threshold of 11 keV. This low threshold is set by x rays from cosmogenic activities. Using 1 t of 86% enriched Ge detectors, the target mass is large enough for dark matter studies. In fact, a 40 kg ^{nat}Ge proof-of-principle experiment has been approved for dark matter studies.

5.1.4. MAJORANA The Majorana proposal (121) (named in honor of Ettore Majorana) involves many of the IGEX collaborators. Their analysis indicated that ^{68}Ge contained within the Ge detectors was the limiting background for their $\beta\beta(0\nu)$ search. (Contrast this with the GENIUS approach described above.) The proposal's design therefore emphasizes segmentation and pulse-shape discrimination to reject this background. The electron capture of ^{68}Ge is not a significant problem, but ^{68}Ge decays to the β^+ emitting ^{68}Ga. This isotope can create background in the $\beta\beta(0\nu)$ window if one of the annihilation gamma rays converts within the crystal. The energy deposits of the positron and gamma ray may pollute the peak window in energy, but the deposits will be separated in space. In contrast, a $\beta\beta(0\nu)$ event will have a localized energy deposit. Segmentation of the crystals permits a veto of such events. Furthermore, distinct ionization events will have a different pulse shape than a localized event. Therefore, pulse-shape analysis can also help reject background. Majorana plans to use 210 86% enriched, segmented Ge crystals for a total of 500 kg of detector. The cryostat would be formed from very pure electroformed Cu ($<$25 μBq/kg ^{226}Ra, 9 μBq/kg ^{228}Th) (87).

5.1.5. MOON The MOON (Mo Observatory of Neutrinos) proposal (122) would use ^{100}Mo as a $\beta\beta(0\nu)$ source and as a target for solar neutrinos. This dual purpose and a sensitivity to low-energy supernova electron neutrinos (128) make it an enticing idea. ^{100}Mo has a high Q-value (3.034 MeV), which results in a large phase-space factor and places the $\beta\beta(0\nu)$ peak region well above most radioactive backgrounds. It also has hints of a favorable $|M^{0\nu}|$ but unfortunately it has a fast $T^{2\nu}_{1/2}$. The experiment will make energy and angular correlation studies to select $\beta\beta(0\nu)$ events and to reject backgrounds. The planned MOON configuration is a supermodule of scintillator and Mo ensembles. One option is a module of plastic fiber scintillators with thin (0.03 g/cm^2) layers of clad Mo, which are arranged to achieve a position resolution comparable to the fiber diameter (2–3 mm). A total of 34 tons of natural Mo would be required.

As a solar neutrino detector, ^{100}Mo has a low threshold of 168 keV, and the estimated observed event rate is $\approx$160/(ton ^{100}Mo $\cdot$ year) without neutrino oscillations. It is sobering to realize that the primary background for the delayed-coincidence solar neutrino signal is accidental coincidences between $\beta\beta(2\nu)$ decays.

The project needs Mo and scintillator radioactive impurity levels of better than 1 mBq/ton, which can be achieved by carbonyl chemistry for Mo while plastics can be produced cleanly. However, the total surface area of the Mo-scintillator modules is $\approx$26000 m^2. Dust, being electrostatically charged, tends to garner Rn daughters and becomes radioactive. Keeping these surfaces clean of dust during production and assembly will be a challenge. Liquid scintillator and bolometer options that would avoid this large surface area are also being considered. The simulations of the design indicate that the energy resolution for the $\beta\beta(0\nu)$ peak will be $\approx$7%, which is at the upper end of the range of feasibility for a sub-50 meV $\langle m_\nu \rangle$ experiment. The bolometer option would also remove the resolution concerns. Use of enriched ^{100}Mo is feasible and would reduce the total volume of

the detector and source ensemble, lowering the internal radioactivity contribution to the background by an order of magnitude.

5.1.6. OTHER PROPOSALS Table 5 summarizes the other proposals of which we are aware. The CAMEO proposal (114) would use 1000 kg of scintillating $^{116}CdWO_4$ crystals situated within the Borexino apparatus. The Borexino liquid scintillator would provide shielding from external radioactivity and light piping of crystal events to the photomultiplier tube array surrounding the system. Early phases of the program would use the Borexino counting test facility. Similarly, the CANDLES proposal (115) (CAlcium fluoride for study of Neutrino and Dark matter by Low-Energy Spectrometer) would immerse CaF_2 in liquid scintillator. The scintillation light from the double beta decay of ^{48}Ca would be detected via photomultiplier tubes. The low isotopic abundance (0.187%) of ^{48}Ca requires a very large operating mass. Two groups (119, 120) have been studying the use of GSO crystals (Gd_2SiO_5:Ce) for the study of ^{160}Gd.

COBRA (CdTe O neutrino double Beta Research Apparatus) (111) would use CdTe or CdZnTe semiconductors to search for $\beta\beta(0\nu)$ in either Cd or Te. Sixteen hundred 1 cm^3 crystals would provide 10 kg of material. The GEM (Germanium Experiment for neutrino Mass) proposal (117) is very similar to the GENIUS proposal, but much of the LN shielding would be replaced with high-purity water.

The Drift Chamber Beta-ray Analyzer (DCBA) proposal (112) is for a three-dimensional tracking chamber in a uniform magnetic field. A drift chamber inside a solenoid and cosmic-ray veto counters comprise the detector. Thin plates of Nd would form the source. The series of NEMO experiments is progressing, with NEMO-3 (113) beginning operation in 2002. In concept, the detector is similar to NEMO-2. That is, it contains a source foil enclosed between tracking chambers that is itself enclosed within a scintillator array. NEMO-3 can contain a total of 10 kg of source and plans to operate with several different isotopes, ^{100}Mo being the most massive at 7 kg. The collaboration is also discussing the possibility of building a 100 kg experiment that would be called NEMO-4.

Two additional groups are proposing to use ^{136}Xe to study $\beta\beta(0\nu)$. Caccianiga & Giammarchi (123) propose to dissolve 1.56 t of enriched Xe in liquid scintillator. The XMASS (124) collaboration proposes to use 10 t of liquid Xe for solar neutrino studies. The detector would have sensitivity to $\beta\beta(0\nu)$.

5.1.7. ISOTOPE ENRICHMENT Only the enrichment facilities of Russia can enrich materials in the 1-ton quantities that are required for the future proposals described above. One of Russia's several centrifuge enrichment facilities, the Electro Chemical Plant (ECP) in Krasnoyarsk, can produce ≈30 kg/y of enriched ^{76}Ge material in apparatus never used for uranium enrichment. With some modest improvements, ECP could increase production to ≈200 kg/y. The ^{136}Xe production rate at these facilities is estimated to be 2 t/y. With several plants throughout Russia and fairly easy expansion, the total capacity is large enough that two samples of isotope could be produced simultaneously.

6. CONCLUSIONS

We have reviewed the motivation, present status, and future plans of the search for $\beta\beta(0\nu)$ decay. Seeing $\beta\beta(0\nu)$ decay would be a remarkable physics result, with important consequences for neutrino physics in particular and for the hunt for physics beyond the standard model in general.

For $N = 3$ neutrino flavors and mass states, the neutrino mass matrix contains, in general, nine parameters. Three mixing angles, two Δm^2 mass differences, and one *CP*-violation phase can be, in principle, determined in neutrino oscillation experiments. Remarkable progress has been made lately in determining some of these parameters, and great effort is being devoted to verify the discoveries already made and to refine and extend the search for neutrino oscillations.

The remaining parameters of the neutrino mass matrix, the absolute mass scale and the two Majorana phases, can be determined or severely constrained only by the observation of $\beta\beta(0\nu)$ decay and/or by further progress in the tritium endpoint neutrino mass experiments. Thus, the search for the $\beta\beta(0\nu)$ decay has become one of the critical issues of particle physics today.

We note again that if a nonzero m_ν is observed in either $\beta\beta(0\nu)$ decay or in tritium beta decay (or, ideally, in both), the nuclear matrix element $|M^{0\nu}|$ issue will become critical. To dramatize this problem, consider the following possibility. Suppose a nonzero $\langle m_\nu \rangle$ of about 100 meV is indicated by an upcoming ^{76}Ge experiment. The anticipated experimental uncertainty is approximately ± 25 meV, and the matrix element uncertainty of a factor of 2–3 would dominate the total uncertainty on the mass parameter. Hence, the possible range of effective neutrino mass would be $33\ \text{meV} < \langle m_\nu \rangle < 300\ \text{meV}$. If one keeps this in mind while looking at the right-hand side of Figure 3, one sees that this matrix element uncertainty alone is large enough to compromise physics conclusions regarding the mass hierarchy at small minimum neutrino masses. We hope that the improved sensitivity of the upcoming $\beta\beta(0\nu)$ experiments will promote an increased interest in the nuclear theory of double beta decay.

The recent neutrino physics results have stimulated a great rebirth of interest in the field of double beta decay. The oscillation experiments indicate that neutrinos do have mass and, in particular, at least one neutrino has a mass greater than $m_{\text{scale}} \approx 50$ meV. The upcoming $\beta\beta(0\nu)$ experiments will have a sensitivity to $\langle m_\nu \rangle$ values below this critical mass scale. This is a very exciting time for $\beta\beta(0\nu)$ research, as it is reasonable to hope for a positive result within the coming decade.

ACKNOWLEDGMENTS

We would like to thank the following colleagues for useful discussions concerning this manuscript: Frank Avignone III, Laura Baudis, John Beacom, Peter Doe, Hiro Ejiri, Giorgio Gratta, Ryuta Hazama, Harry Miley, and Michael Moe.

This work was supported by the U.S. Department of Energy under contracts DEFG03-97ER41020 and DE-FG03-88ER40397.

LITERATURE CITED

1. Moe M, Vogel P. *Annu. Rev. Nucl. Part. Sci.* 44:247 (1994)
2. Kajita T, Totsuka Y. *Rev. Mod. Phys.* 73: 85 (2001)
3. Ahn SH, et al. *Phys. Lett.* B511:178 (2001)
4. Fukuda Y, et al. *Phys. Lett.* B335:237 (1994)
5. Becker-Szendy RA, et al. *Phys. Rev.* D46:3720 (1992)
6. Allison WWM, et al. *Phys. Lett.* B449:137 (1999)
7. Cleveland BT, et al. *Astrophys. J.* 496:505 (1998)
8. Ahmad QR, et al. *Phys. Rev. Lett.* 87: 071301 (2001); *Phys. Rev. Lett.* 89: 001301 (2002); *Phys. Rev. Lett*. 001302 (2002)
9. Fukuda S, et al. *Phys. Rev. Lett.* 86:5651 (2001); *Phys. Rev. Lett* 86:5656 (2001)
10. Hampel W, et al. *Phys. Lett.* B447:127 (1999)
11. Abdurahitov JN, et al. *Phys. Rev. C* 60:055801 (1999)
12. Apollonio M, et al. *Phys. Lett.* B466:415 (1999)
13. Boehm F, et al. *Phys. Rev. D* 64:112001 (2001)
14. Chikige Y, Mohapatra RN, Peccei RD. *Phys. Lett.* B98:265 (1981)
15. Racah G. *Nuovo Cim.* 14:322 (1937)
16. Majorana E. *Nuovo Cim.* 14:171 (1937)
17. Goeppert-Mayer M. *Phys. Rev.* 48:512 (1935)
18. Furry WH. *Phys. Rev.* 56:1184 (1939)
19. Primakoff H, Rosen SP. *Rep. Progr. Phys.* 22:121 (1959)
20. Haxton WC, Stephenson GJ, Jr. *Progr. Part. Nucl. Phys.* 12:409 (1984)
21. Doi M, Kotani T, Takasugi E. *Progr. Theor. Phys. Suppl.* 83:1 (1985)
22. Boehm F, Vogel P. *Physics of Massive Neutrinos.* Cambridge, UK: Cambridge Univ. Press (1992). 2nd ed.
23. Suhonen J, Civitarese O. *Phys. Rep.* 300: 123 (1998)
24. Faessler A, Šimkovic F. *J. Phys. G* 24: 2139 (1998)
25. Vergados JD. *Phys. Atom. Nucl.* 63:1137 (2000)
26. Klapdor-Kleingrothaus HV. *Springer Tracts in Mod. Phys.* 163:69 (2000)
27. Tretyak VI, Zdesenko YuG. *At. Data Nucl. Data Tables* 61:43 (1995)
28. Tretyak VI, Zdesenko YuG. *At. Data Nucl. Data Tables* 80:83 (2002)
29. Groom DE, et al. *Eur. J. Phys. C* 15:1 (2000)
30. Fisher P, Kayser B, McFarland KS. *Annu. Rev. Nucl. Part. Sci.* 49:481 (1999)
31. Kobzarev IYu, et al. *Sov. J. Nucl. Phys.* 32:823 (1980)
32. Kayser B, Gibrat-Debu F, Perrier F. *The Physics of Massive Neutrinos.* Singapore: World Sci. (1985)
33. Zralek M. *Acta Phys. Pol.* B28:2225 (1997)
34. Yanagida T. *Proc. Workshop on Unified Theory*, ed. Sawada and Sugamoto, KEK, (1979); Gell-Mann M, Ramond P, Slansky R. *Supergravity*, ed. P van Nieuwenhuizen, DZ Freedman. Amsterdam: North Holland (1979)
35. Li LF, Wilczek F. *Phys. Rev. D* 25:143 (1982); Kayser B, Shrock RE. *Phys. Lett.* B112:137 (1982); Kayser B. *Phys. Rev. D* 26:1662 (1982)
36. Paes H, Hirsch M, Klapdor-Kleingrothaus HV, Kovalenko SG. *Phys. Lett.* B453:194 (1999); *Phys. Lett.* B498:35 (2001)
37. Schechter J, Valle JWF. *Phys. Rev. D* 25:2951 (1982)
38. Doi M, et al. *Phys. Lett.* B102:323 (1981)

39. Wolfenstein L. *Phys. Lett.* B107:77 (1981)
40. Zee A. *Phys. Lett.* B93:389 (1980); *Phys. Lett.* B161:141 (1985)
41. Vissani F. *JHEP* 06:022 (1999)
42. Bilenky SM, et al. *Phys. Lett.* B465:193 (1999); Bilenky SM, Pascoli S, Petcov ST. *Phys. Rev. D* 64:053010 (2001)
43. Klapdor-Kleingrothaus HV, Pas H, Smirnov AY. *Phys. Rev. D* 63:073005 (2001)
44. Matsuda K, et al. *Phys. Rev. D* 64:013001 (2001)
45. Czakon M, et al. *Phys. Rev. D* 65:053008 (2001)
46. Pascoli S, Petcov ST, Wolfenstein L. *Phys. Lett.* B524:319 (2002)
47. Feruglio F, Strumia A, Vissani F. hep-ph/0201291
48. Zuber K. hep-ph/0008080
49. Kaulard J, et al. *Phys. Lett.* B422:334 (1998)
50. Appel R, et al. *Phys. Rev. Lett.* 85:2877 (2000)
51. Littenberg LS, Shrock R. *Phys. Lett.* B491:255 (2000)
52. Weinheimer Ch, et al. *Phys. Lett.* B460:219 (1999)
53. Lobashev VM, et al. *Phys. Lett.* B460:227 (1999)
54. Vogel P, Ericson M, Vergados JD. *Phys. Lett.* B212:259 (1988); Muto K. *Phys. Lett.* B277:13 (1992)
55. Balysh A, et al. *Phys. Rev. Lett.* 77:5186 (1996)
56. Brudanin VB, et al. *Phys. Lett.* B495:63 (2000)
57. Klapdor-Kleingrothaus HV, et al. *Eur. Phys. J. A* 12:147 (2001)
58. Avignone FT, et al. *Phys. Lett.* B256:559 (1991)
59. Aalseth CE, et al. *Nucl. Phys.* B48:223 (Proc. Supp.) (1996)
60. Elliott SR, et al. *Phys. Rev. C* 46:1535 (1992)
61. Arnold R, et al. *Nucl. Phys.* A636:209 (1998)
62. Arnold R, et al. *Nucl. Phys.* A658:299 (1999)
63. Kawashima A, Takahashi K, Masuda A. *Phys. Rev. C* 47:2452 (1993)
64. Wieser ME, De-Laeter JR. *Phys. Rev. C* 64:024308 (2001)
65. Dassie D, et al. *Phys. Rev. D* 51:2090 (1995)
66. Ejiri H, et al. *Phys. Lett.* B258:17 (1991)
67. Ejiri H, et al. *J. Phys. G* 17:S155 (1991)
68. De Silva A, Moe MK, Nelson MA, Vient MA. *Phys. Rev. C* 56:2451 (1997)
69. Alston-Garnjost M, et al. *Phys. Rev. C* 55:474 (1997)
70. Ashitkov VD, et al. *JETP Lett.* 74:529 (2001)
71. Vasil'ev SI, et al. *JETP Lett.* 51:622 (1990)
72. Arnold R, et al. *Z. Phys. C* 72:239 (1996)
73. Danevich FA, et al. *Phys. Rev. C* 62:044501 (2000)
74. Ejiri H, et al. *J. Phys. Soc. Jpn.* 64:339 (1995)
75. Bernatowicz T, et al. *Phys. Rev. C* 47:806 (1993)
76. da Cruz MTF, et al. *Phys. Rev. C* 48:3106 (1993)
77. Gavriljuk JuM, et al. *Phys. Rev. C* 61:035501 (2000)
78. Artemiev V, et al. *Phys. Lett.* B345:564 (1995)
79. Turkevich AL, Economou TE, Cowan GA. *Phys. Rev. Lett.* 67:3211 (1991)
80. Caurier E, Nowacki F, Poves A, Retamosa J. *Phys. Rev. Lett.* 77:1954 (1996); Caurier E, Nowacki F, Poves A, Retamosa J. *Nucl. Phys.* A654:973c (1999)
81. Engel J, Vogel P, Zirnbauer M. *Phys. Rev. C* 37:731 (1988)
82. Staudt A, Muto K, Klapdor-Kleingrothaus HV. *Europhys. Lett.* 13:31 (1990)
83. Toivanen J, Suhonen J. *Phys. Rev. Lett.* 75:410 (1995)
84. Pantis G, Šimkovic F, Vergados JD, Faessler A. *Phys. Rev. C* 53:695 (1996)
85. Moe M. *Nucl. Phys.* B (Proc. Suppl.) 19:158 (1991)
86. Benziger JB, et al. *Nucl. Instrum. Methods A* 417:278 (1998)
87. Brodzinski RL, Miley HS, Reeves JH,

Avignone FT. *Nucl. Instrum. Methods A* 292:337 (1990)
88. Boger J, et al. *Nucl. Instrum. Methods A* 449:172 (2000)
89. Wang YF, et al. *Phys. Rev. D* 64:013012 (2001)
90. Abdurashitov J, et al. physics/0001007
91. Macdonald B, Diaz JA, Kaplan SN, Pyle RV. *Phys. Rev.* 139:B1253 (1965)
92. Kozlowski T, et al. *Nucl. Phys.* A436:717 (1985)
93. O'Connell JS, Schima FJ. *Phys. Rev. D* 38:2277 (1988)
94. Moe MK. *Phys. Rev. C* 44:R931 (1991); Barabash AS, et al. *Phys. Lett.* B345:408 (1995)
95. Barabash AS, et al. *Phys. At. Nucl.* 62: 2039 (1999)
96. De Braeckeleer L, et al. *Phys. Rev. Lett.* 86:3510 (2001)
97. Griffiths A, Vogel P. *Phys. Rev. C* 46:181 (1992)
98. You Ke, et al. *Phys. Lett.* B265:53 (1991)
99. Aalseth CE, et al. *Phys. Rev. C* 59:2108 (1999); *Nucl. Phys. Russ. Acad. Sci.* 63: 1299 (2000); hep-ex/0202026
100. Ejiri H, et al. *Phys. Rev. C* 63:065501 (2001)
101. Alessandrello A, et al. *Phys. Lett.* B486:13 (2000)
102. Luescher R, et al. *Phys. Lett.* B434:407 (1998)
103. Barabash AS. *Phys. Lett.* B216:257 (1989)
104. Baudis L, et al. *Phys. Rev. Lett.* 83:41 (1999)
105. Avignone FT III, et al. *Nucl. Phys.* B (Proc. Suppl.) 28A:280 (1992)
106. Klapdor-Kleingrothaus HV, Dietz A, Harney HL, Krivosheina IV. *Mod. Phys. Lett.* 16:2409 (2001)
107. Aalseth, et al. hep-ex/0202018
108. Elliott SR, Hahn AA, Moe MK. *Phys. Rev. Lett.* 59:2020 (1987)
109. Elliott SR, Hahn AA, Moe MK. *Nucl. Instrum. Methods A* 273:226 (1988)
110. Arnold R, et al. *Nucl. Phys.* A678:341 (2000)
111. Zuber K. *Phys. Lett.* B519:1 (2001)
112. Ishihara N, et al. *Nucl. Instrum. Methods A* 443:101 (2000)
113. Sarazin X, et al. hep-ex/0006031
114. Bellini G, et al. *Eur. Phys. J. C* 19:43 (2001)
115. Kishimoto T, et al. *Osaka University Laboratory for Nuclear Studies Annual Report* (2000)
116. Avignone FT, et al. hep-ex/0201038
117. Zdesenko YuG, Ponkratenko OA, Tretyak VI. *J. Phys.* G27:2129 (2001)
118. Klapdor-Kleingrothaus HV. hep-ph/ 0103074
119. Danevich FA, et al. *Nucl. Phys.* A694:375 (2001)
120. Wang SC, Wong HT, Fujiwara M. hep-ex/ 0009014. Submitted to *Astropart. Phys.*
121. Aalseth CE, et al. hep-ex/0201021
122. Ejiri H, et al. *Phys. Rev. Lett.* 85:2917 (2000)
123. Caccianiga B, Giammarchi MG. *Astropart. Phys.* 14:15 (2001)
124. Moriyama S, et al. Presented at XENON01 Workshop, Dec. 2001, Tokyo, Jpn.
125. Pirro S, et al. *Nucl. Instrum. Methods A* 444:71 (2000)
126. Danilov M, et al. *Phys. Lett.* B480:12 (2000)
127. Klapdor-Kleingrothaus HV, Hellmig J, Hirsch M. *J. Phys.* G24:483 (1998)
128. Ejiri H, Engel J, Kudomi N. *Phys. Lett.* B530:27 (2002)

Annual Review of Nuclear and Particle Science
Volume 52, 2002

CONTENTS